


ORIGINAL RESEARCH

# Sodium-Glucose Cotransporter 2 Inhibitor Canagliflozin Antagonizes Salt-Sensitive Hypertension Through Modifying Transient Receptor Potential Channels 3 Mediated Vascular Calcium Handling

Yu Zhao, MS; Li Li, MD; Zongshi Lu, MD; Yingru Hu, MS; Hexuan Zhang, MS; Fang Sun, MD; Qiang Li, MD; Chengkang He, MD; Wentao Shu, MS; Lijuan Wang, BS; Tingbing Cao, BS; Zhidan Luo, MD; Zhencheng Yan, MD; Daoyan Liu, PhD; Peng Gao, PhD; Zhiming Zhu , MD

**BACKGROUND:** Salt-sensitive hypertension is highly prevalent and associated with cardiorenal damage. Large clinical trials have demonstrated that SGLT2 (sodium-glucose cotransporter 2) inhibitors exert hypotensive effect and cardiorenal protective benefits in patients with hypertension with and without diabetes. However, the underlying mechanism remains elusive.

**METHODS AND RESULTS:** Dahl salt-sensitive rats and salt-insensitive controls were fed with 8% high-salt diet and some of them were treated with canagliflozin. The blood pressure, urinary sodium excretion, and vascular function were detected. Transient receptor potential channel 3 (TRPC3) knockout mice were used to explain the mechanism. Canagliflozin treatment significantly reduced high-salt-induced hypertension and this effect was not totally dependent on urinary sodium excretion in salt-sensitive hypertensive rats. Assay of vascular function and proteomics showed that canagliflozin significantly inhibited vascular cytoplasmic calcium increase and vasoconstriction in response to high-salt diet. High salt intake increased vascular expression of TRPC3 in salt-sensitive rats, which could be alleviated by canagliflozin treatment. Overexpression of TRPC3 mimicked salt-induced vascular cytosolic calcium increase in vitro and knockout of TRPC3 erased the antihypertensive effect of canagliflozin. Mechanistically, high-salt-induced activation of NCX1 (sodium-calcium exchanger 1) reverse mode increased cytoplasmic calcium level and vasoconstriction, which required TRPC3, and this process could be blocked by canagliflozin.

**CONCLUSIONS:** We define a previously unrecognized role of TRPC3/NCX1 mediated vascular calcium dysfunction in the development of high-salt-induced hypertension, which can be improved by canagliflozin treatment. This pathway is potentially a novel therapeutic target to antagonize salt-sensitive hypertension.

**Key Words:** NCX1 ■ salt-sensitive hypertension ■ SGLT2 inhibitor ■ TRPC3 ■ vasocontraction

See Editorial by Yagi and Kolluru

**C**ardiovascular disease has always been the biggest threat to human health.<sup>1</sup> Chronic vascular diseases such as hypertension and atherosclerosis are the main pathogenic factors or early pathological

processes of high-mortality diseases such as coronary heart disease, myocardial infarction, and heart failure. High salt intake not only acts as an independent risk factor for hypertension but also causes cardiovascular

Correspondence to: Zhiming Zhu, MD, and Peng Gao, PhD, Department of Hypertension and Endocrinology, Center for Hypertension and Metabolic Diseases, Daping Hospital, Army Medical University, Chongqing Institute of Hypertension, Chongqing 400042, China. Email: [hbpems@sina.com](mailto:hbpems@sina.com) and [gaopengscu@aliyun.com](mailto:gaopengscu@aliyun.com)

Supplemental Material is available at <https://www.ahajournals.org/doi/suppl/10.1161/JAHA.121.025328>

For Sources of Funding and Disclosures, see page 16.

© 2022 The Authors. Published on behalf of the American Heart Association, Inc., by Wiley. This is an open access article under the terms of the [Creative Commons Attribution-NonCommercial-NoDerivs](https://creativecommons.org/licenses/by-nc-nd/4.0/) License, which permits use and distribution in any medium, provided the original work is properly cited, the use is non-commercial and no modifications or adaptations are made.

JAHA is available at: [www.ahajournals.org/journal/jaha](http://www.ahajournals.org/journal/jaha)

## CLINICAL PERSPECTIVE

### What Is New?

- The SGLT2 (sodium-glucose cotransporter 2) inhibitor canagliflozin antagonizes salt-induced hypertension in salt-sensitive rats by directly alleviating vasoconstriction.
- Salt-induced vascular transient receptor potential channel 3 upregulation results in an augmented vasoconstriction in salt-sensitive hypertensive rats through facilitating NCX1 (sodium-calcium exchanger 1)-mediated vascular calcium uptake, which could be alleviated by canagliflozin.

### What Are the Clinical Implications?

- Antagonizing the interaction between transient receptor potential channel 3 and NCX1 by the SGLT2 inhibitor canagliflozin would represent a novel target to antagonize salt-sensitive hypertension.
- Canagliflozin exerts its antihypertensive effect beyond its canonical effect on renal natriuresis.

## Nonstandard Abbreviations and Acronyms

<b>[Ca<sup>2+</sup>]<sub>cyt</sub></b>	cytosolic free calcium concentration
<b>NCX1</b>	sodium-calcium exchanger 1
<b>ND</b>	normal diet
<b>SGLT2i</b>	sodium-glucose exchanger 2 inhibitor
<b>SS</b>	Dahl salt-sensitive rats
<b>SS-19BN</b>	Dahl salt-insensitive rats
<b>TRPC3</b>	transient receptor potential channels 3

and renal damage.<sup>2,3</sup> High salt intake raises blood pressure (BP) through activation of the sympathetic nerve system and renin-angiotensin system and leads to renal sodium retention.<sup>4</sup> Modest reduction in dietary salt intake substantially reduces cardiovascular events in the general population, but daily salt intake has remained unchanged in the past 2 decades.<sup>5,6</sup> Thus, to identify an alternative therapy for reducing the detrimental effect of high salt is critical for the treatment of salt-sensitive hypertension.

Recently, a new series of antidiabetic drugs, SGLT2 (sodium-glucose cotransporter 2) inhibitors (SGLT2i), including canagliflozin, dapagliflozin, and empagliflozin, display impressive renal and cardiovascular benefits and reduce all-cause and cardiovascular death in patients with and without diabetes from several large-scale clinical trials.<sup>7–10</sup> The potential mechanisms that

account for the cardio-beneficial effect of SGLT2i might include lowering plasma volume, lowering blood glucose, increasing urinary sodium excretion, and reducing renin-angiotensin system activation, all of which might help to lower BP.<sup>11</sup> However, it remains elusive whether SGLT2i might directly act on vascular function and BP.

Vascular smooth muscle contraction is evoked by an increase in cytosolic free calcium concentration ( $[Ca^{2+}]_{cyt}$ ), promoting actin-myosin cross-bridge formation.<sup>12</sup> Vasoconstriction is also regulated by several calcium-dependent mechanisms involving voltage dependent calcium channel, receptor coupled intracellular calcium release from store,<sup>13,14</sup> NCX (sodium-calcium exchanger) as well as calcium signaling related proteins,<sup>15,16</sup> such as CamKII. Canonical transient receptor potential channels (TRPCs) and NCX1 have also been shown to play a role in altered calcium handling and vascular dysfunction in hypertension.<sup>17,18</sup> Several studies showed that TRPC3 mediates cell membrane depolarization and regulates vasoconstriction.<sup>19–23</sup> Our previous study showed that TRPC3 contributes to raised  $[Ca^{2+}]_{cyt}$  and high BP in both hypertensive rats and patients,<sup>24,25</sup> which can be upregulated by high salt intake.<sup>26,27</sup> However, cardiovascular damage induced by high salt in response to TRPC3 needs further confirmation. It is also unknown whether the antihypertensive effects of SGLT2i depend on the regulation of the vascular calcium homeostasis.

In this study, we investigated the potential mechanism underlying the hypotensive effect of SGLT2i and examined whether SGLT2i can be used for treatment of salt-sensitive hypertension. We provided ample evidence showing that TRPC3 was a critical target of SGLT2i that regulates the vascular function and calcium handling. Our results revealed a previous unrecognized role of SGLT2i in the management of hypertension.

## METHODS

### Availability of Data and Materials

All data and materials are available upon request.

### Animals and Treatment

Six-week-old male Dahl salt-sensitive rats (SS), which are commonly used to investigate the mechanisms contributing to salt-sensitive hypertension,<sup>28,29</sup> and Dahl salt-insensitive rats (SS-19<sup>BN</sup>) were obtained from Vital River Company, Beijing, China (Table S1) and housed under controlled temperature (21–23 °C) with a 12/12 hour light–dark cycle with free access to food and water. After a 1-week adaptation period, 24 male SS rats and 24 age-matched SS-19<sup>BN</sup> were randomly divided into normal diet group (ND) and others were randomly assigned to 2 groups: the high-salt group

(HS, high-salt chow containing 8% (w/w) NaCl) and the high-salt plus canagliflozin group (HS+canagliflozin, 8% NaCl chow and 20mg/kg per day canagliflozin in drinking waters). Every week the tail-cuff BP levels were measured. After 12 weeks, the rats were surgically measured for 24-hour ambulatory BP levels and carotid pressure. Then, euthanasia was performed by exsanguination under overdose of anesthetic gas (isoflurane 5%), and tissue samples were isolated for further experiments.

Wild-type (WT) and *Trpc3*<sup>-/-</sup> mice were purchased from the Jackson Laboratory (B6;129S mice, Bar Harbor, ME, Table S1). Homozygotes, heterozygotes, and WT littermates were identified according to previously described methods.<sup>24</sup> Briefly 30 8-week-old *Trpc3*<sup>-/-</sup> mice and 30 8-week-old WT littermates were randomly divided into normal diet group and other animals were randomly assigned to HS and HS+canagliflozin groups. Every week the tail-cuff BP levels were measured. Echocardiography was performed using a high-resolution in vivo micro-imaging system Vevo-770 (Visual Sonics, USA) with a real-time micro visualization scan head of 17.5MHz. After 24 weeks of intervention, these animals were euthanized by overdose of anesthetic gas (isoflurane 5%) followed by exsanguination, and tissue samples were isolated for other experiments.

All experimental procedures were performed in accordance with protocols approved by the Institutional Animal Care and Use Committee of the Army Medical University.

### Tail-Cuff and 24-Hour Ambulatory BP Measurements

The tail-cuff BP measurement was conducted using a Softron BP-2010A as previously described.<sup>24,25,27</sup> The 24-hour ambulatory BP measurement was conducted as previously described using surgically implanted telemetric transmitters (Data Sciences International, New Brighton, MN). The rats were anesthetized by gaseous anesthesia (isoflurane 4% for induction and 1.2–2.5% for maintenance), and the implant catheter was placed into the abdominal aorta of rats. The animals were allowed to recover from the surgery for at least 7 days, and the 24-hour ambulatory systolic and diastolic BP were then measured by telemetry in conscious, unrestrained animals. We collected data once every minute and used the mean values of 24 hours for the analysis.

### Measurement of Biochemical and Electrolyte of Urine and Serum

Rats were placed in individual metabolic cages (Tecniplast, Italy) for 24 hours, and during the experiment, they had ad libitum access to food and water. Total urine was collected, and urinary sodium

and potassium excretion concentration was measured using an electrolyte detector (XI-921 Analyzer, Shenzhen, China). Urine and serum creatinine levels were measured in the same samples using the colorimetric creatine assay kit from Abcam (Cambridge, MA) according to the manufacturer's instruction. Blood urea nitrogen was assayed using the urea assay kit from Sigma-Aldrich according to the manufacturer's instruction. Blood sodium and potassium excretion concentration was also measured using an electrolyte detector (XI-921 Analyzer, Shenzhen, China). Blood glucose was monitored by the Nova StatStrip Xpress glucometer (Nova Biomedical, Waltham, MA) by cutting the tail and gently massaging blood onto a glucose test strip. The plasma H<sub>2</sub>S content was measured by free radical analyzer TBR4100 with an H<sub>2</sub>S-selective sensor (World Precision Instruments, China) as previously described.<sup>30</sup> Arterial nitric oxide concentration was measured by Micro NO Content Assay Kit (Solarbio, Beijing, China).

### Measurement of Vascular Reactivity

The vascular reactivity was measured as previously described.<sup>24</sup> Briefly after the mice or rats were anesthetized with pentobarbital sodium, the mesenteric vascular bed was removed and placed in cold (4 °C) Krebs solution (in mmol/L: 118 NaCl, 25 NaHCO<sub>3</sub>, 11 D-glucose, 4.7 KCl, 1.2 KH<sub>2</sub>PO<sub>4</sub>, 1.17 MgSO<sub>4</sub>, and 2.5 CaCl<sub>2</sub>, set to the pH of 7.4). The first branches of the mesenteric arteries (Mas) (for mice) and second branches of the Mas (for rats) were excised with the connective tissues, such as fat. Subsequently, 2-mm MA segments were mounted on a myograph (Danish Myo Technology, Aarhus, Denmark). After incubation in 95% O<sub>2</sub> and 5% CO<sub>2</sub> at 37 °C, the MA segments were stretched to optimum baseline tension (1.8mN for mouse Mas and 2.5mN for rat Mas). The arteries were then equilibrated for 60 minutes before precontraction with 60mmol/L KCl. After several washouts, each ring was treated with different vasoactive substances (phenylephrine, U46619, acetylcholine, or nitroglycerin, purchased from Sigma-Aldrich) or other substances (Pyr3, canagliflozin, SN6, KB-R7943, purchased from Sigma-Aldrich or MedChemExpress, USA). All substances were dissolved in DMSO at a final concentration of 0.1%, and an equal amount of DMSO was negative control. Isometric contractions were recorded using a computerized data acquisition system (Power Lab/8SP; AD Instruments Pty Ltd, Castle Hill, Australia).

### Vascular Smooth Muscle Cell Culture and Transfection

The vascular smooth muscle cells (Mouse aortic VSMCs, purchased from Procell Company, China) were cultured at 37 °C and 5% CO<sub>2</sub> in Dulbecco's modified Eagle's medium supplemented with 10%

fetal bovine serum, streptomycin (100  $\mu\text{g}/\text{mL}$ ) and penicillin (100U/mL). This control medium was used as the standard control medium and the HS medium was made by adding 20mmol/L NaCl as previously described.<sup>27,31</sup> The VSMCs were typically subjected to fetal bovine serum-free control or HS medium for 24 hours. All substances (Pyr3, canagliflozin, SN6, KB-R7943) were dissolved in DMSO and preincubated for 30 minutes before HS treatment, and an equal amount of DMSO was negative control.

Plasmid overexpression and knockdown experiments were conducted as previously described.<sup>24</sup> Briefly, Lipofectamine 3000 was purchased from Thermo Fisher Scientific (Waltham, MA), and the mice TRPC3 overexpression and knockdown plasmid was ordered from Genechem Co., Ltd (Shanghai, China).

### Intracellular Calcium Measurement

The cytosolic  $\text{Ca}^{2+}$  concentrations were measured using Fura-2 AM (ThermoFisher Scientific, Waltham, MA), respectively.<sup>24,26</sup> For the  $[\text{Ca}^{2+}]_{\text{cyt}}$  measurement, cells were digested and resuspended in Hank's Balanced Salt Solution (in mmol/L: 136 NaCl, 5.4 KCl, 0.44  $\text{KH}_2\text{PO}_4$ , 0.34  $\text{Na}_2\text{HPO}_4$ , 5.6 D-glucose, 10 HEPES and 1  $\text{CaCl}_2$ , pH 7.4). For loading with Fura-2, the cells were incubated with 1  $\mu\text{mol}/\text{L}$  Fura-2 AM and 0.025% F-127 (from Sigma-Aldrich) for 30 minutes at 37 °C in the dark, washed 3 times with  $\text{Ca}^{2+}$ -free Hank's Balanced Salt Solution and resuspended in  $\text{Ca}^{2+}$ -free Hank's Balanced Salt Solution. Fluorescence was measured at baseline and after treatment at an emission of 510nm using excitation wavelengths of 340 and 380nm. The resultant data are presented as  $F_x/F_0$ , where  $F_x$  is the ratio of fluorescence between excitation at 340 and 380nm with emission at 510nm, and  $F_0$  is the mean F340/F380nm value during the pretreatment period in each experiment. Changes in  $[\text{Ca}^{2+}]_{\text{cyt}}$  were deduced from the ratios of the transient increases in the fluorescence intensity at 340 and 380nm. To visualize the staining, the specimens were placed on an inverted fluorescence microscope (Nikon TE-2000, Nikon Corporation, Tokyo, Japan).

### Immunofluorescence and Histological Examination

Immunofluorescence studies were performed using frozen sections of MAs (10 $\mu\text{m}$ ) that were fixed and incubated with mouse anti-NCX1-specific polyclonal antibody (Abcam), rabbit anti-TRPC3-specific polyclonal antibody (Alomone, Jerusalem, Israel) overnight at 4 °C. The section of MAs was then incubated for 30 minutes with fluorescent dye-labeled secondary antibodies (Invitrogen, USA) at 37 °C. Subsequently, the sections were imaged and analyzed using a fluorescence microscope (Nikon ECLIPSE Ti2, Japan).

Slides of formalin-fixed, paraffin-embedded MAs were stained with hematoxylin and eosin. Microscopic visualization and photographs were obtained, and the measurements of wall thickness, lumen diameter, and the ratio of artery wall to the lumen were performed by a blinded investigator using NIS-Elements software (Nikon, Tokyo, Japan).

### iTRAQ Quantitative Proteomics

The BIOTREE company (Shanghai, China) performed the tandem mass tag based proteomics analysis of aortic tissue of SS. Each group has 3 samples. The procedures used are described elsewhere.<sup>32–34</sup> The aorta tissue has been reported to partially reflect the changes in resistant arteries.<sup>35</sup> In brief, 200mg aortic tissue per sample was obtained from SS in each group. The proteins from each sample were precipitated with acetone and redissolved in the triethylammonium bicarbonate buffer. Then, proteins were quantified by BCA protein assay kit (no. p0010, Beyotime) and about 100  $\mu\text{g}$  of proteins were digested to peptides. The peptides were further labeled with the iTRAQ tags (Applied Biosystems) and analyzed by online electrospray tandem mass spectrometry. It was performed on a Nano Aquity UPLC system (Waters Corporation) that was connected to an LTQ Orbitrap XL mass spectrometer (Thermo Fisher Scientific) equipped with an online nanoelectrospray ion source (Michrom Bioresources). Proteins identified by 2 or more unique peptides were taken for further analysis. Differentially expressed proteins were selected according to a 2-fold change (fold change <0.83 or >1.2). The gene ontology annotation (<http://www.geneontology.org/>) was used to annotate the function of proteins. Enriched pathways were analyzed by the Kyoto Encyclopedia of Genes and Genomes database (<http://www.kegg.jp/kegg/pathway.html>). A 2-tailed Fisher's exact test was used in the gene ontology Kyoto Encyclopedia of Genes and Genomes enrichment analyses.  $P < 0.05$  was considered significant.

### Western Blot and Reverse Transcription Polymerase Chain Reaction

For western blot assays, the primary antibody against TRPC3 was purchased from Alomone (Alomone Labs), and the primary antibody against MYPT1 and phosphorylated MYPT1 was purchased from Santa Cruz Biotechnology (Dallas, TX). The primary antibody against phosphorylated CamkII, MLC2, phosphorylated MLC2, and  $\beta$ -actin was purchased from Cell Signaling Technology (Danvers, MA, USA). Primary antibodies against NCX1 and CamkII were purchased from Abcam. The source and dilution of antibodies were shown in Table S2. Horseradish peroxidase-labeled secondary antibodies were purchased from

Zhongshan Company (Beijing, China). Data were normalized to  $\beta$ -actin.

For reverse transcription polymerase chain reaction, total RNA was isolated from MAs and VSMCs using Trizol (Invitrogen, Carlsbad, CA). First strand cDNA was synthesized using random primers and M-MuLV Reverse Transcriptase (Transcriptor First Strand cDNA Synthesis Kit, Roche). Polymerase chain reactions were carried out with the manufacturer (Light Cycler 96, Roche), using the QuantiTect SYBR Green RT-PCR Kit (Roche). Light Cycler analysis software (LightCycler® 96 software, Roche) was used to determine crossing points using the second derivative method. Data were normalized to housekeeping genes (GAPDH).

### Immunoprecipitation

Immunoprecipitation was performed as previously described protocol.<sup>36</sup> RIPA buffer (1% Triton-X, 0.1% SDS, 0.5% deoxycholate, 50 mmol/L Tris pH7.5, 150 mmol/L NaCl, protease inhibitor; Roche) was used for lysis and immunoprecipitation. Briefly, tissue or podocytes lysates were precleared with Dynabeads Protein A for 20 minutes. Control immunoprecipitation was performed using equal amount of rabbit IgG. The lysate was incubated with TRPC3 or NCX1 antibody overnight at 4 °C, followed by 4 hours in the presence of Dynabeads Protein A. Beads were washed 6 times in lysis buffer, and proteins were eluted with Laemmli loading buffer by boiled at 65 °C for 25 minutes to prevent precipitation of the transmembrane proteins. Then elution was analyzed by western blotting for TRPC3 or NCX1. Primary antibodies against NCX1 were purchased from ProteinTech Group (Chicago, IL) and the primary antibody against TRPC3 was purchased from Alomone (Alomone Labs).

### Statistical Analysis

Data are expressed as mean $\pm$ SEM. Unpaired Student *t* test and 1-way ANOVA were used to perform statistical analysis in this study. All experiments were repeated at least 3 times, and representative experiments are shown. Statistical significance was achieved when  $P < 0.05$ .

## RESULTS

### Canagliflozin Treatment Antagonizes Salt-Sensitive Hypertension and Vascular Remodeling

First, we determined the effect of canagliflozin on salt-sensitive hypertension using SS and their SS-19<sup>BN</sup> controls. Tail-cuff results indicate that high salt intake significantly induced an elevation of systolic BP in SS but did not affect BP in SS-19<sup>BN</sup> (Figure 1A).

Administration of canagliflozin for 3 months lowered BP in SS but not in SS-19<sup>BN</sup> (Figure 1A). The results of 24-hour ambulatory BP monitoring and invasively measured carotid artery BP also confirm an antihypertensive effect of canagliflozin in SS (Figure 1B, Figure S1A and S1B).

As sympathetic nerve activation and renal sodium retention are associated with salt-sensitive hypertension, we detected heart rate and plasma electrolyte and found that both parameters were unchanged with or without canagliflozin treatment (Figure S1C and S1D). As expected, canagliflozin treatment significantly reduced body weight and blood glucose level, accompanied with a remarkable increase of urinary glucose excretion, in both SS and SS-19<sup>BN</sup> (Figure S1E, S1F, and S1L), resulting in an equal blood glucose level between SS and SS-19<sup>BN</sup>. As the antihypertensive effect of SGLT2 inhibitor might also depend on its promotional effect on urinary sodium excretion, we also measured renal function and urinary electrolyte level. High salt diet significantly impaired renal function, as evidenced by decreased creatinine clearance and elevated blood urea nitrogen level, especially in SS (Figure S1G and S1H). Canagliflozin displayed an obvious protective effect on renal function, but the creatinine clearance in SS remained lower than that of SS-19<sup>BN</sup> after canagliflozin treatment (Figure S1G and S1H). However, canagliflozin significantly promoted urinary sodium excretion without affecting potassium excretion in both groups of rats, resulting in an equal amount of urinary sodium excretion between the 2 groups (Figures S1I through S1K). The expression level of renal Na-Cl cotransporter, which contributes to salt-sensitive hypertension by promoting renal sodium and potassium reabsorption,<sup>37</sup> was increased in response to HS diet but not affected by canagliflozin (Figure S1M). These results indicate that although the renal function of SS had not totally recovered, the plasma and urinary sodium and glucose levels were almost equal between the 2 groups after canagliflozin treatment, implying that the antihypertensive effect of canagliflozin might not only rely on its promotional effect on urinary sodium excretion and renal function.

Next, we showed that high salt intake significantly promoted the vascular remodeling with higher thickness of medial layer and less lumen diameter in SS compared with SS-19<sup>BN</sup> (Figure 1C). Importantly, canagliflozin treatment remarkably alleviated HS-induced vascular remodeling in SS (Figure 1C). To clarify how high salt intake regulates the vasculature of salt-sensitive hypertension, the aortas of SS were analyzed by proteomics. The upregulated expressed proteins in response to HS diet were mainly enriched in vasoconstriction and calcium transport related signaling pathways (Figure 1D). In a consistent, gene ontology analysis also showed that high salt intake increased a large number of proteins

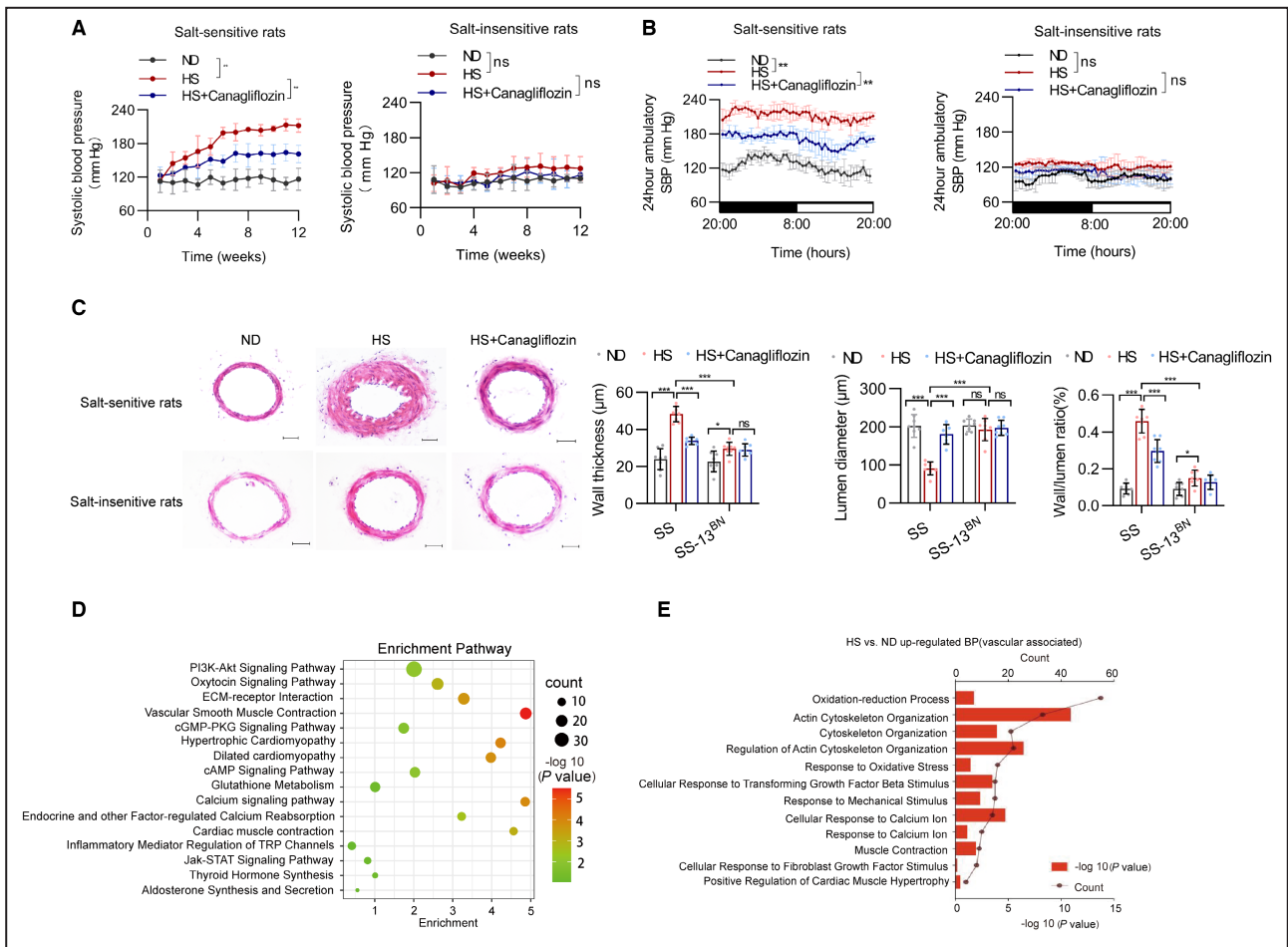


**Figure 1. Effects of canagliflozin on vasculature from Dahl salt-sensitive and Dahl salt-insensitive rats.**

**A**, The time course of systolic blood pressure in Dahl salt-sensitive and Dahl salt-insensitive rats fed with a normal diet, high-salt diet (8% NaCl) and high-salt diet plus canagliflozin (8% salt+20mg/kg/d canagliflozin) for 12 weeks. n=8. **B**, SBP from 24-hour blood pressure was determined using radiotelemetry at 12th week in Dahl salt-sensitive and Dahl salt-insensitive rats. n=8. **C**, Representative images of hematoxylin–eosin staining cross-sections of mesenteric arteries isolated from Dahl salt-sensitive and Dahl salt-insensitive rats. Statistical analysis of mesenteric artery wall thickness, lumen diameter, and the ratio of artery wall to the lumen. n=8. Scale bar denotes 25 µm. **D**, The upregulated KEGG pathways enriched by differentially expressed proteins in groups between ND and HS. **E**, The vascular-associated biological process terms (GO) enriched by upregulated proteins in groups between ND and HS. Results are expressed as mean±SEM. Statistical significance was determined by unpaired Student *t* test. A 2-tailed Fisher’s exact test was used in the GO KEGG enrichment analyses. \**P*<0.05, \*\**P*<0.01, \*\*\**P*<0.001, ns, no significant difference. ECM indicates extracellular matrix; GO, gene ontology; HS, high-salt diet; KEGG, Kyoto Encyclopedia of Genes and Genomes; ND, normal diet; SBP, systolic blood pressure; SS, Dahl salt-sensitive rats; SS-13<sup>BN</sup>, Dahl salt-insensitive rats; and TRP, transient receptor potential.

associated with vasoconstriction and calcium transport (Figure 1E). These results suggest that there existed a local impact of canagliflozin on vasculature itself, in which vascular contraction and related calcium signaling pathway might be involved.

### Beneficial Effect of Canagliflozin on Vascular Dysfunction and Calcium Handling

As microvascular vasodilation and vasoconstriction play an important role in the regulation of BP, we investigated the vascular reactivity in isolated MAs from SS and SS-19<sup>BN</sup>. Chronic HS diet reduced endothelium-dependent

and endothelium-independent vasodilation in both SS and SS-19<sup>BN</sup>, and canagliflozin treatment improved endothelium-dependent vasodilation and endothelium-independent vasodilation in both SS and SS-19<sup>BN</sup> (Figure S2A and S2B). However, there was no significant difference of vasodilatation between SS and SS-19<sup>BN</sup> with or without canagliflozin treatment (Figure S2A and S2B). The plasma levels of vascular regulatory gasotransmitters, such as H<sub>2</sub>S and nitric oxide, were significantly reduced by HS diet but not affected by canagliflozin in SS (Figure S2C and S2D). To define the direct effects of canagliflozin in the vasculature of salt-sensitive hypertension, we investigated the direct effect of canagliflozin on the vascular reactivity in isolated MAs from SS.

It showed that acute canagliflozin treatment caused endothelium-dependent relaxation, but acute canagliflozin treatment did not improve endothelium-independent relaxation (Figure S2E). On the other hand, long-term HS diet increased phenylephrine- or U46619-induced vasoconstriction in SS, and this promotional effect of salt was significantly inhibited by canagliflozin (Figure 2A and 2B). In addition, canagliflozin incubation also significantly inhibited phenylephrine- or U46619-induced constriction of isolated arteries from SS on HS diet compared with those on normal diet (Figure 2C). Moreover, the inhibitory effect of canagliflozin is not regulated by nitric oxide treated with a nitric oxide blocker L-name (Figure 2D). These results imply that the antihypertensive effect of canagliflozin on SS mainly relied on vasoconstriction but not vasodilatation even though endothelial function was also improved.

Next, cytosolic calcium level was detected using a calcium sensitive fluorescent dye in cultured mouse VSMCs as the increased cytoplasmic calcium level contributes to vasoconstriction. And canagliflozin significantly blocked the promotional effect of HS medium on cytosolic calcium uptake following transglutaminase-mediated endoplasmic reticulum calcium release (Figure 2E and 2F). These results suggest a critical role of vascular calcium handling in the therapeutic effect of canagliflozin on salt-sensitive hypertension.

### Canagliflozin Reduced Proteins Related to the Vascular Contraction and Calcium Signaling Pathway in Response to High Salt

To determine how canagliflozin regulates vascular dysfunction, the aortas of SS receiving canagliflozin were analyzed via proteomics. Venn diagram identified 627 proteins that were upregulated by high salt intake and downregulated by canagliflozin (Figure 3A). Kyoto Encyclopedia of Genes and Genomes analysis revealed that the downregulated proteins affected by canagliflozin were mainly enriched in the regulation of actin cytoskeleton and vasoconstriction (Figure 3B). In GO analysis, canagliflozin mainly affected proteins that related to actin cytoskeleton organization, calcium response, and cytoplasmic calcium uptake (Figure 3C and 3D).

Next, we asked which molecule participated in the regulatory effect of canagliflozin on vascular calcium handling. As our previous studies found that sodium permeable cation channel TRPC3 increased the cytosolic calcium and vasoconstriction,<sup>24,25</sup> the expression of TRPC3 was detected in aortas of rats. HS diet increased the vascular protein expression level of TRPC3 and NCX1, a sodium/calcium exchanger, in SS, as well as increased CamKII proteins that related to calcium handling (Figure 3E). All these changes were alleviated by canagliflozin (Figure 3E). In addition, canagliflozin

also reduced HS-induced phosphorylation of vascular MYPT1 and MLC2 proteins that directly contributes to the vasoconstriction (Figure 3F). However, vascular TRPC3 and phosphorylation of MYPT1 and MLC2 proteins were not significant difference in SS-19<sup>BN</sup> (Figure 3F). In vascular smooth muscle cells, the expression of TRPC3, NCX1, and CAMKII was increased in response to HS medium. In contrast, canagliflozin inhibited the increased expression of TRPC3, NCX1, and CAMKII induced by HS medium, which was not significantly suppressed in normal salt medium (Figure S2F). These results suggest that TRPC3 might be a critical target of canagliflozin in antagonizing salt-sensitive hypertension.

### TRPC3 Mediated Calcium Handling is a Target for Canagliflozin

To further demonstrate how TRPC3 contribute to HS-induced calcium handling and vasoconstriction, immunofluorescent staining was performed on mesenteric artery slices. The results showed that TRPC3 and NCX1 were colocalized in the medial layer and their expression level in SS was significantly increased by high salt intake and attenuated by canagliflozin treatment (Figure 4A). However, in SS-19<sup>BN</sup>, although the expression of NCX1 was also significantly increased by high salt, the expression of TRPC3 was not remarkably changed (Figure 4A). In cultured mouse VSMC, overexpression of TRPC3 by plasmid transfection increased transglutaminase-mediated endoplasmic reticulum calcium release and cytosolic calcium level, all of which were significantly reduced by knockdown of TRPC3 (Figure S3A). Accordingly, high sodium treatment increased the cytoplasmic calcium level, which was further aggravated by TRPC3 overexpression and attenuated by TRPC3 knockdown (Figure 4B). Importantly, canagliflozin treatment reduced the cytoplasmic calcium level, but this effect was reversed by silencing TRPC3 (Figure 4B). Similarly, the cytosolic calcium increase was also enhanced in response to high sodium and reduced by canagliflozin in a TRPC3-dependent manner (Figure 4C). Moreover, intracellular calcium flow and cytoplasmic calcium concentration were correlated with TRPC3 mRNA level (Figure S3B and S3C). These results support that TRPC3 is a key target for high sodium mediated the vascular calcium dysregulation, which can be modified by canagliflozin. To investigate the relationship between TRPC3 and vasoconstriction, we assayed the contraction of MAs of SS in response to TRPC3 inhibitors. Inhibition of TRPC3 by Pyr3 potently suppressed the HS-induced vasoconstriction compared with control group (Figure 4D). Importantly, overexpression of TRPC3 gene also increased CamKII and phosphorylation of CamKII protein expression in cultured VSMCs, which could be

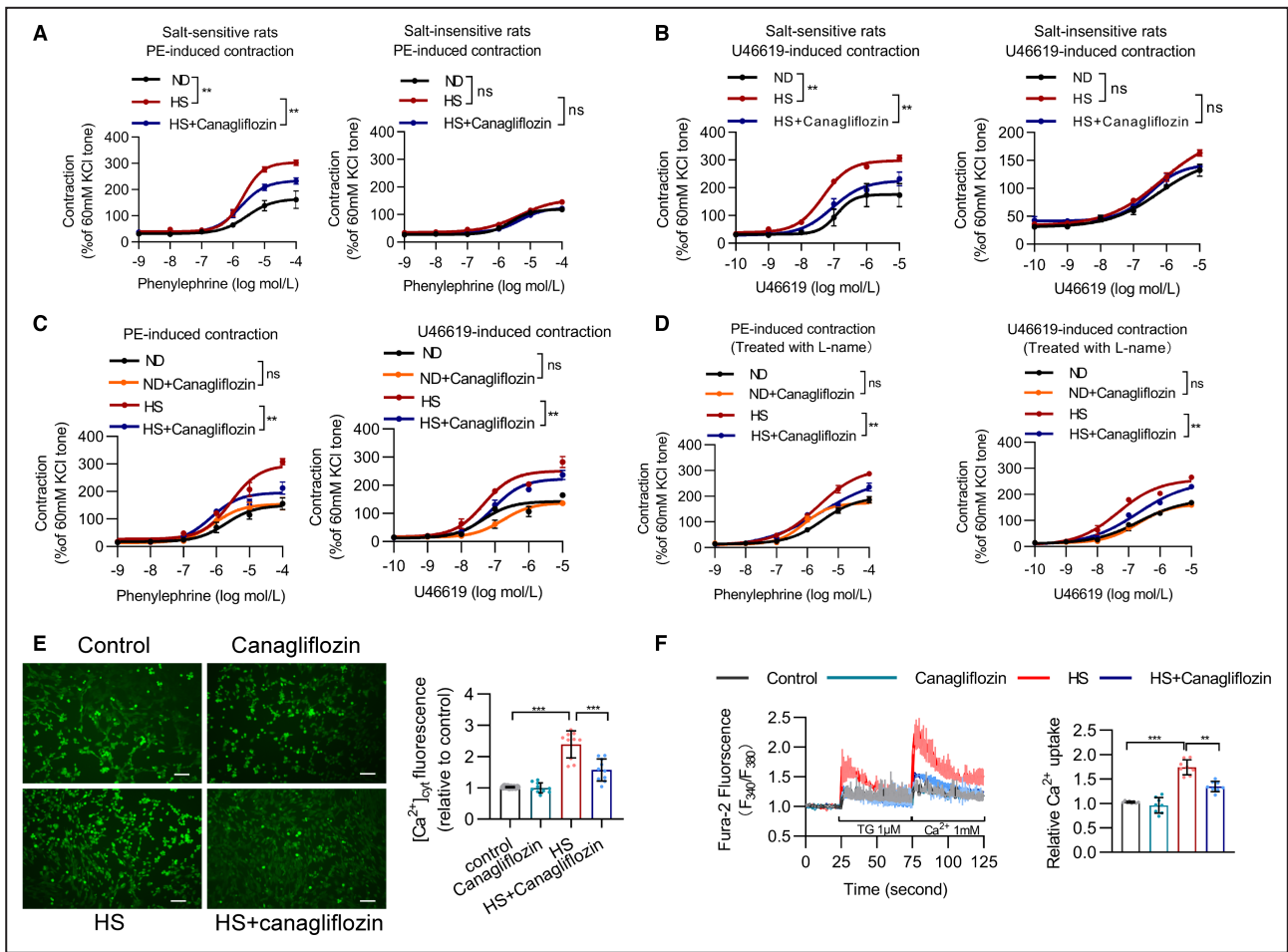


**Figure 2. Direct effect of canagliflozin on vasoconstriction and calcium uptake.**

**A**, PE-induced vasoconstriction of the mesenteric artery rings from Dahl salt-sensitive and Dahl salt-insensitive rats. *n*=8. **B**, U46619-induced vasoconstriction of the mesenteric artery rings from Dahl salt-sensitive and Dahl salt-insensitive rats. *n*=8. **C**, Effect of acute canagliflozin (10 μmol/L) preincubation on U46619- or PE-induced vasoconstriction of the mesenteric artery rings from Dahl salt-sensitive rats. *N*=8. **D**, Effect of acute canagliflozin and L-name (100 μmol/L) preincubation on U46619- or PE-induced vasoconstriction of the mesenteric artery rings from Dahl salt-sensitive rats. *N*=8. **E**, Effects of high salt and canagliflozin on cytosolic calcium imaging. The relative fluorescence intensity of the mouse vascular smooth muscle cells (VSMCs) treated with control, HS (20 mmol/L NaCl), canagliflozin (10 μmol/L canagliflozin), and HS+canagliflozin (20 mmol/L NaCl+10 μmol/L canagliflozin) were quantified. *n*=12. **F**, Cytosolic Ca<sup>2+</sup> concentrations ([Ca<sup>2+</sup>]<sub>cyt</sub>) in thapsigargin-induced endoplasmic reticulum (ER) Ca<sup>2+</sup> release and Ca<sup>2+</sup> uptake via store operated channels (SOCs) after ER Ca<sup>2+</sup> depletion in mouse VSMCs treated with control, canagliflozin, HS, and HS+canagliflozin. Cells were incubated in a Ca<sup>2+</sup>-free buffer in the presence of Fura-2 (1 μmol/L). Peak F<sub>x</sub>/F<sub>0</sub> following thapsigargin (1 mmol/L, TG) stimulation and after reintroducing 100 μmol/L extracellular Ca<sup>2+</sup>. [Ca<sup>2+</sup>]<sub>cyt</sub> was monitored by Fura-2 fluorescence at F340 and F380 nm. The quantitative results are shown on the right. *n*=12. Results are expressed as mean±SEM. Statistical significance was determined by unpaired Student *t* test for comparisons between 2 groups and 1-way ANOVA followed by Bonferroni's posttest for multiple comparisons. \*\**P*<0.01, \*\*\**P*<0.001. HS indicates high-salt diet; ND, normal diet; PE, phenylephrine; SS, Dahl salt-sensitive rats; and SS-13BN, Dahl salt-insensitive rats.

blocked by either canagliflozin or silencing of TRPC3 (Figure 4E), suggesting that TRPC3 plays a critical role in the vascular calcium handling and function, especially under HS intervention.

### TRPC3 Knockout Alleviated HS-Induced Vasoconstriction and Hypertension

To validate the role of TRPC3 in HS-induced hypertension, TRPC3 knockout mice and littermate WT mice

were fed with HS diet, and accompanied by canagliflozin treatment. In WT mice, high salt intake significantly increased systolic BP for about 40 mmHg after 6-month treatment (Figure 5A and 5B). Compared with their WT littermates, TRPC3 knockout mice displayed a much lower systolic BP after salt loading (Figure 5A and 5B). Accordingly, HS-induced vascular remodeling was also attenuated in TRPC3 knockout mice, as evidenced by decreasing vascular wall thickening and luminal diameter (Figure 5C). Importantly, TRPC3



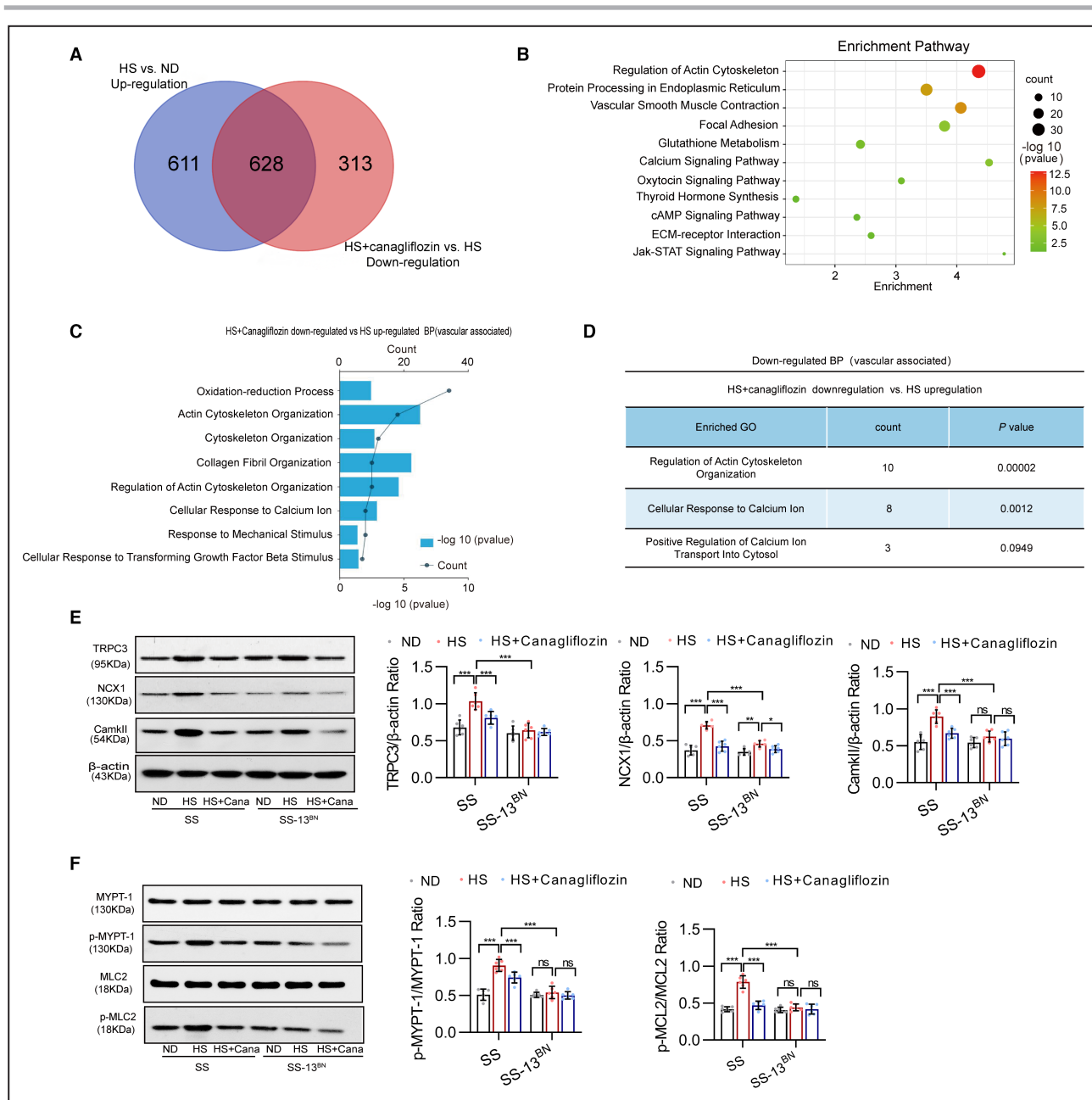


**Figure 3. Canagliflozin inhibited the vascular contraction and calcium channel-related protein pathways.**

**A**, Venn diagram in groups between upregulated proteins of ND vs HS and downregulated proteins of HS vs HS+canagliflozin. **B**, The KEGG pathways enriched by differentially expressed proteins in groups between upregulated proteins of ND vs HS and downregulated proteins of HS vs HS+canagliflozin. **C** and **D**, The vascular-associated biological process terms (GO) enriched by differentially expressed proteins in groups between upregulated proteins of ND vs HS and down-regulated proteins of HS vs HS+canagliflozin. **E** and **F**, Representative western blots of TRPC3, NCX1, CamkII, MYPT-1, MLC2, and phosphorylation of MYPT-1 and MLC2 (p-MYPT-1 and p-MLC2) in carotid artery from Dahl salt-sensitive and Dahl salt-insensitive rats.  $\beta$ -actin served as a loading control. n=8. Results are expressed as mean $\pm$ SEM. Statistical significance was determined by unpaired Student *t* test for comparisons between 2 groups and 1-way ANOVA followed by Bonferroni's posttest for multiple comparisons. A 2-tailed Fisher's exact test was used in the GO KEGG enrichment analyses. \**P*<0.05, \*\**P*<0.01, \*\*\**P*<0.001. ECM, extracellular matrix; GO, gene ontology; HS, high-salt diet; KEGG, Kyoto Encyclopedia of Genes and Genomes; NCX1, sodium-calcium exchanger 1; ND, normal diet; SS, Dahl salt-sensitive rats; SS-13BN, Dahl salt-insensitive rats; and TRPC3, transient receptor potential channels 3.

knockout abolished the inhibitory effect of canagliflozin on HS-induced hypertension or vascular remodeling (Figure 5C). After canagliflozin treatment, there were no differences between endothelium-dependent and

endothelium-independent relaxation in WT and TRPC3 knockout mice (Figure S3D and S3E). However, phenylephrine- or U46619-induced vasoconstriction was lower in TRPC3 knockout mice compared with WT

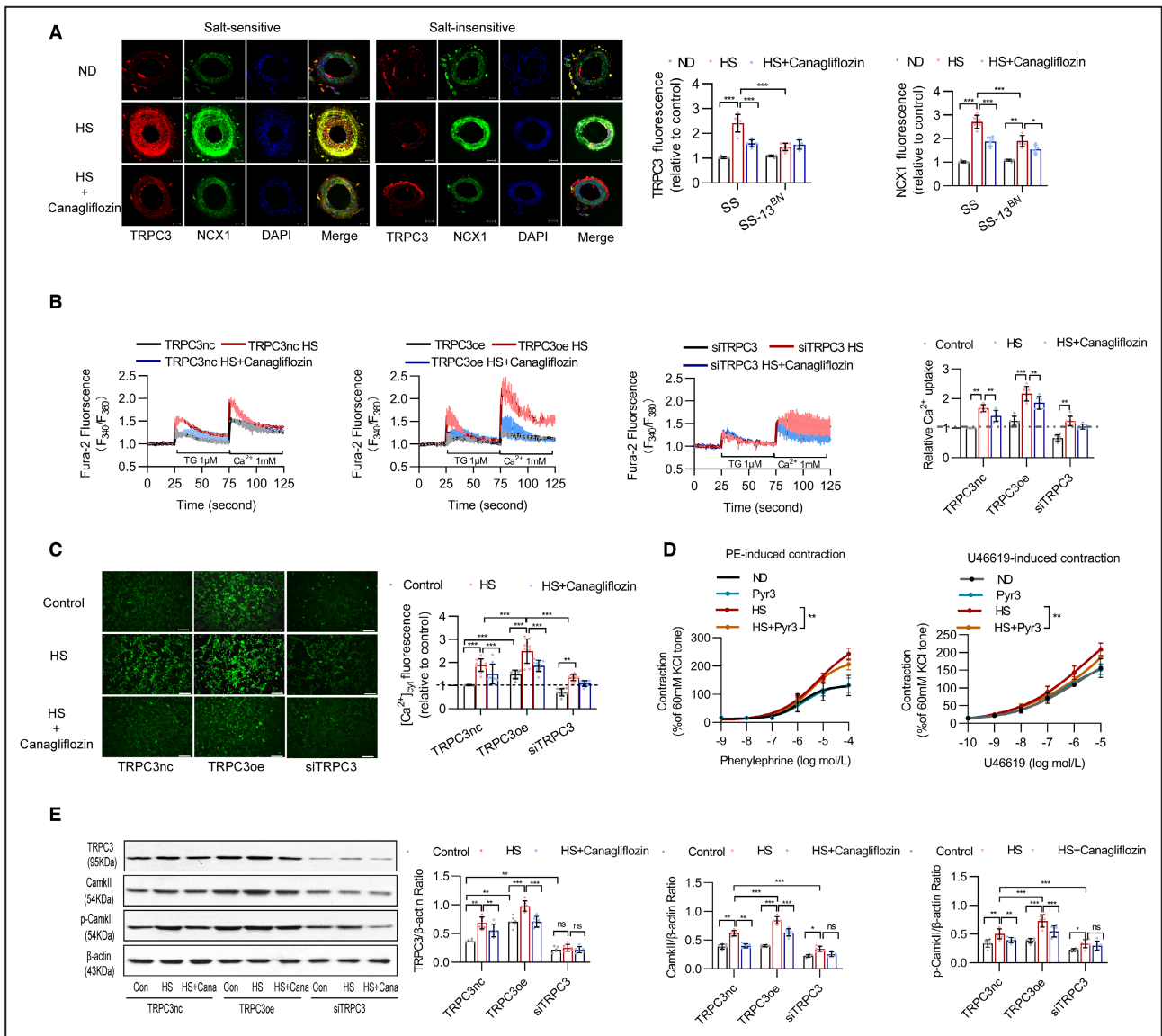


**Figure 4. Canagliflozin regulated calcium influx in vascular smooth muscle cells mediated by TRPC3.**

**A**, Representative images of the immunofluorescence staining of TRPC3, NCX1, and DAPI using mesenteric arteries isolated from Dahl salt-sensitive and Dahl salt-insensitive rats. Bar represents 25  $\mu$ m. Quantification of the intensities in each graph was presented in the right 2 panels. n=8. **B**, [Ca<sup>2+</sup>]<sub>cyt</sub> in ER Ca<sup>2+</sup> release and Ca<sup>2+</sup> uptake in mouse VSMCs transferred with TRPC3-nc, TRPC3-oe, and si-TRPC3 plasmids and treated with control, HS, and HS+canagliflozin. The quantitative results are shown on the right. n=12. **C**, Cytosolic calcium imaging of VSMCs transferred with TRPC3-nc, TRPC3-oe, and si-TRPC3 plasmids and treated with control, HS, and HS+canagliflozin, The relative fluorescence intensity of VSMCs were quantified. n=12. **D**, Effect of acute Pyr3 (TRPC3 inhibitor, 10  $\mu$ mol/L) preincubation on PE- and U46619-induced vasoconstriction of the mesenteric artery rings from Dahl salt-sensitive fed with ND and HS. n=8. **E**, Representative western blots of TRPC3, CamkII, and phosphorylation of CamkII in mouse VSMCs transferred with TRPC3-nc, TRPC3-oe, and si-TRPC3 plasmids and treated with control (Con), HS, and HS+canagliflozin (HS+Cana).  $\beta$ -actin served as a loading control. n=8. Results are expressed as mean $\pm$ SEM. Statistical significance was determined by unpaired Student *t* test for comparisons between 2 groups and 1-way ANOVA followed by Bonferroni's posttest for multiple comparisons. \**P*<0.05, \*\**P*<0.01, \*\*\**P*<0.001. ER indicates endoplasmic reticulum; HS, high-salt diet; NCX1, sodium-calcium exchanger 1; ND, normal diet; PE, phenylephrine; si-TRPC3, TRPC3 silence; SS, Dahl salt-sensitive rats; SS-13BN, Dahl salt-insensitive rats; TRPC3, transient receptor potential channels 3; TRPC3-nc, TRPC3 negative control; TRPC3-oe, TRPC3 overexpression; and VSMC, vascular smooth muscle cell.

mice. TRPC3 knockout also attenuated HS-induced vasoconstriction and reduced the inhibitory effect of canagliflozin on vasoconstriction (Figure 5D and 5E). In consistence, the inhibitory effects of canagliflozin on

HS-induced myocardial hypertrophy and dysfunction, as evidenced by decreased ejection fraction, were also blocked in TRPC3 knockout mice (Figure S3F through S3I).

To further determine the interaction between TRPC3 and NCX1 *in vivo*, immunofluorescent staining was performed in MAs from TRPC3 knockout mice. Like SS, a remarkable increase of fluorescent signal of both TRPC3 and NCX1 was found in the sections of WT mice with high salt intake, which was decreased by canagliflozin treatment. However, these effects were rarely detected in TRPC3 knockout mice (Figure 5F). Similar to immunofluorescent staining results, the inhibitory effects of canagliflozin on HS-induced increase of the vascular CamkII, TRPC3, and NCX1 protein levels or phosphorylation of MYPT1 and MLC2 were remarkably reduced in TRPC3 knockout mice (Figure 5G and 5H). These results suggest that there exists a potential interaction between TRPC3 and NCX1 in response to salt loading and canagliflozin and canagliflozin might regulate NCX1 in a TRPC3-dependent manner.

### Canagliflozin Exerted Its Effect Through Inhibition of Binding of TRPC3-NCX1 Complex

To explore whether the interaction between TRPC3 and NCX1 participates in the regulatory effect of high salt intake on vasoconstriction, inhibitors of TRPC3 or NCX1 were applied in artery ring test. Either TRPC3 inhibitor Pyr3 or NCX1 inhibitor SN6 failed to affect the relaxation of mouse MAs (Figure S4A). However, inhibition of NCX1 remarkably inhibited vasoconstriction, and this effect could be further augmented by TRPC3 inhibitor, suggesting a regulatory effect of TRPC3 on NCX1-mediated vasoconstriction (Figure 6A). In addition, inhibition of NCX1 reduced TRPC3 overexpression-induced cytosolic calcium increase, and this inhibitory effect was attenuated in cultured VSMCs with TRPC3 gene knockdown. (Figure 6B). TRPC3 overexpression also increased both mRNA and protein expression of NCX1 in cultured VSMCs, which could be blocked by either canagliflozin or silencing TRPC3 (Figure 6C and Figure S4B). Furthermore, both NaCl and Na-Gluconate could increase cytoplasmic calcium uptake and upregulate the expression of TRPC3, NCX1, and CAMKII proteins (Figure S4C and S4D). On the other hand, mannitol showed little effect, suggesting that it was the Na<sup>+</sup> ion that regulated the calcium-related proteins expression of TRPC3, NCX1, and CAMKII (Figure S4C and S4D).

Previous studies have demonstrated that activation of the reverse mode of NCX1 contributes to the cytosolic calcium increase in response to high sodium stimulation.<sup>38,39</sup> The inhibitory effect of reverse NCX1 inhibitor KB-R7943 on high-sodium-induced calcium increase was more potent than NCX1 pan inhibitor SN6 (Figure S4E). In addition, the inhibitory effect of KB-R7943 on phenylephrine- or U46619-induced vasoconstriction was stronger than SN6 (Figure 6D).

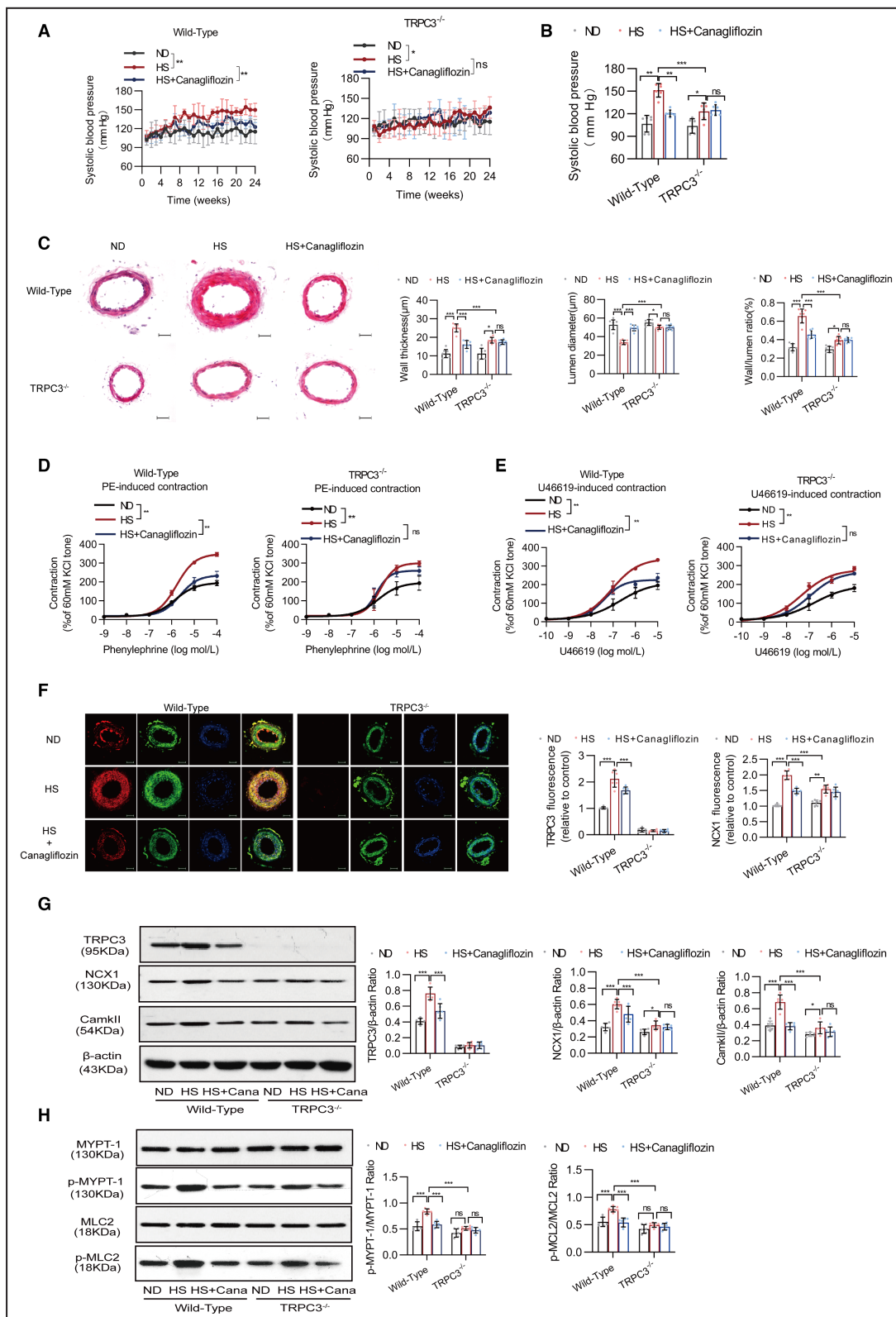
KB-R7943 significantly inhibited high-sodium-induced increase of cytoplasmic calcium levels, whereas this effect was significantly attenuated by normal-sodium medium or knockdown of TRPC3 gene (Figure 6E and 6F), suggesting that the switching of NCX1 to its reverse mode under high salt loading required TRPC3. Accordingly, both TRPC3 inhibitor and NCX1 inhibitor significantly inhibited vasoconstriction in the MAs of WT mice fed with HS diet. By contrast, these inhibitory effects were significantly attenuated in TRPC3 knockout mice (Figure 6G and 6H).

The inhibitory effects of canagliflozin could not be superimposed by PYR3 or KB-R7943 and its effects were comparable to the combination of PYR3 and KB-R7943, suggesting that the inhibitory effect of canagliflozin was mediated by TRPC3 and NCX1 (Figure 6I). Although high-sodium medium directly increased the expression of both TRPC3 and NCX1, the effect of NCX1 inhibitors affected only NCX1 itself, but TRPC3 inhibitor displayed an inhibitory effect on NCX1 expression, suggesting that NCX1 might act as a downstream target of TRPC3 (Figure 6J). Co-immunoprecipitation revealed that high salt promoted the binding of TRPC3 and NCX1, but canagliflozin, TRPC3 inhibitor, or NCX1 inhibitor significantly decreased the interaction between TRPC3 and NCX1 (Figure 6K). These results suggested that increased binding of TRPC3 on NCX1 facilitates the reverse mode switching of NCX1 that mediated the promotional effect of high salt on the vascular calcium handling. Canagliflozin antagonized HS-induced cytoplasmic calcium increase and vasoconstriction by reducing the binding of TRPC3 on mNCX1 (Figure 7).

## DISCUSSION

In this study, we provide novel evidence to demonstrate that TRPC3 is a potential salt-sensitive channel participates in salt-sensitive hypertension. We showed that HS-induced vascular TRPC3 upregulation might account for the augmented vasoconstriction through facilitating the reverse mode switching of NCX1 that promoted vascular calcium handling. Canagliflozin treatment improved the vascular dysfunction and lowered BP through inhibition of TRPC3/NCX1 complex formation in SS with hypertension. This study for the first time revealed a previously unrecognized mechanism responsible for the development of salt sensitivity in the vasculature and highlights a promising role of SGLT2 inhibitor in the treatment of salt-sensitive hypertension.

Salt-sensitive hypertension accounts for 50% to 60% of hypertensive patients. Despite several salt reduction strategies, such as salt-restricted diet and use of diuretics and inhibitors for renin-angiotensin-aldosterone system, HS-induced cardiorenal damage



is still frequent in the population with hypertension.<sup>40</sup> In addition to hypersensitivity of sympathetic nerves, the kidneys display a prominent role in salt-sensitive hypertension by manipulation of sodium balance, as

evidenced by several experimental findings in genetically hypertensive rat strains.<sup>41</sup> Genome-wide association study data also support that possible candidate genes related to salt sensitivity are involved in renal

**Figure 5. Reduction of vasoconstriction by canagliflozin was dependent on TRPC3.**

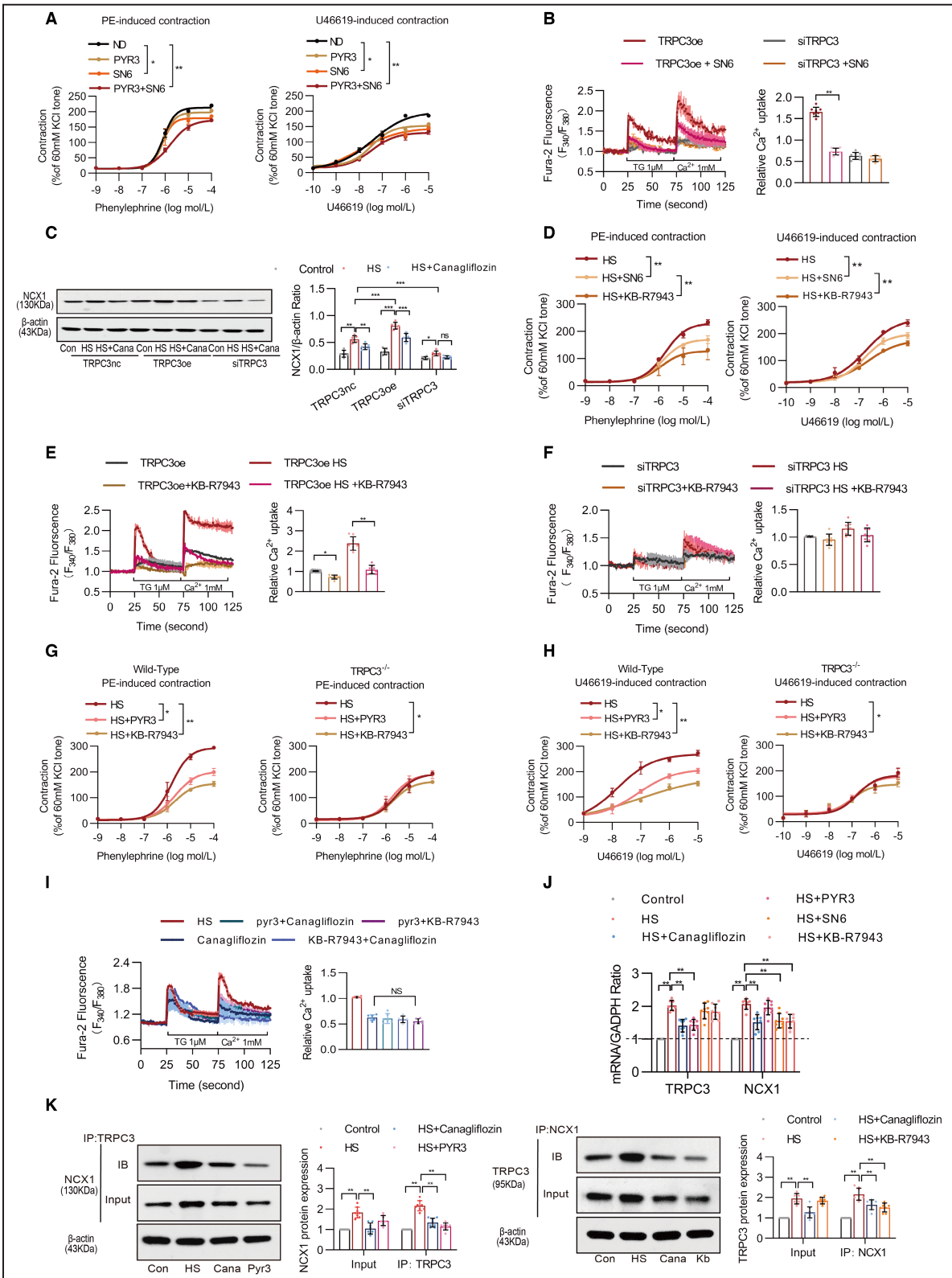
**A**, The time course of SBP in wild-type and TRPC3<sup>-/-</sup> mice fed with ND, HS, and HS+canagliflozin for 24 weeks. n=8. **B**, The 24th week of SBP in wild-type and TRPC3<sup>-/-</sup> mice fed with ND, HS, and HS+canagliflozin for 24 weeks. N=8. **C**, Representative images of hematoxylin–eosin staining cross-sections of mesenteric arteries isolated from wild-type and TRPC3<sup>-/-</sup> mice. Statistical analysis of mesenteric artery wall thickness, lumen diameter, and the ratio of artery wall to the lumen. Scale bar denotes 25 μm. N=8. **D** and **E**, PE- and U46619-induced vasoconstriction of the mesenteric artery rings isolated from wild-type and TRPC3<sup>-/-</sup> mice. n=8. **F**, Representative images of the immunofluorescence staining of TRPC3, NCX1, and DAPI using mesenteric arteries from wild-type and TRPC3<sup>-/-</sup> mice. Bar represents 25 μm. Quantification of the intensities in each graph was presented in the right 2 panels. n=8. **G** and **H**, Representative western blots of TRPC3, NCX1, CamkII, MYPT-1, p-MYPT-1, MLC2, and p-MLC2 in carotid artery from wild-type and TRPC3<sup>-/-</sup> mice fed with ND, HS, and HS+canagliflozin (HS+Cana). β-actin served as a loading control. n=8. Results are expressed as mean±SEM. Statistical significance was determined by unpaired Student *t* test for comparisons between 2 groups and 1-way ANOVA followed by Bonferroni's posttest for multiple comparisons. \**P*<0.05, \*\**P*<0.01, \*\*\**P*<0.001, ns, no significant difference. HS, high-salt diet; NCX1, sodium-calcium exchanger 1; ND, normal diet; PE, phenylephrine; SBP, systolic blood pressure; and TRPC3, transient receptor potential channels 3.

sodium transport.<sup>42</sup> However, in subjects who are salt sensitive, salt-induced increase in renal vascular resistance failed to result in a slower urinary salt excretion compared with normal subjects, and the sodium excretion level among these subjects did not show any difference.<sup>43</sup> Similarly, our study also found that high salt could decrease creatinine clearance and increase urea nitrogen in both SS and SS-19<sup>BN</sup>, whereas the difference in urinary sodium excretion was limited in SS and SS-19<sup>BN</sup> in response to HS diet. These findings suggested that renal mechanism might not be the only reason that accounts for hypertension in SS in the present study. Further we found that HS diet significantly induced vascular remodeling in SS but not SS-19<sup>BN</sup>. In parallel, proteomics on aortic tissue suggested multiple groups of differentially expressed proteins that were enriched in pathways of calcium regulation and vasoconstriction. In addition, MA reactivity assay confirmed that although both endothelium-dependent and endothelium-independent vasodilation were impaired by HS diet, the fact that they happened in the two rat strains indicates that the impaired vasodilation on salt loading would not explain the reason for the enhanced salt sensitivity in SS. However, the phenomenon that the vasoconstriction was enhanced by HS diet existed only in SS, suggesting that enhanced vasoconstriction might be critical for the occurrence of salt-sensitive hypertension.

In recent years, several large clinical trials showed that SGLT2i displayed excellent cardiorenal protective effects in patients with and without diabetes.<sup>7–10</sup> Because SGLT2 mainly locates in the proximal tubules, its lowering BP and cardiorenal protective effect is thought to depend on its role in promoting urinary sodium and glucose excretion and weight loss.<sup>44–46</sup> In this study, canagliflozin significantly reduced BP in SS with hypertension but not in SS-19<sup>BN</sup>. Importantly, the urinary sodium excretion treated by canagliflozin was equivalent in SS and SS-19<sup>BN</sup>, indicating that the antihypertensive effects of canagliflozin involve mechanisms other than natriuresis. Previous studies have found that SGLT2i improve vasodilation in diabetic

and hypertensive rats.<sup>47–50</sup> We also found that canagliflozin could directly cause endothelium-dependent vasodilation. Indeed, canagliflozin significantly improved endothelium-dependent and endothelium-independent vasodilation in both SS and SS-19<sup>BN</sup> but alleviated vasoconstriction only in SS. Furthermore, the proteomic also suggested that canagliflozin downregulated calcium regulated pathways and vasoconstriction pathways in response to the HS diet, indicating that the mechanisms responsible for the antihypertensive effect of canagliflozin contain calcium regulation and vasoconstriction. Therefore, the mechanism accounting for the antihypertensive effect of canagliflozin would be highly overlapped with that of enhanced salt sensitivity in SS.

For investigating the hypotensive mechanism of canagliflozin, the data from proteomics clearly pointed to genes that related to calcium regulatory pathways in the vasculature of SS, suggesting that the abnormal regulation of calcium in cardiovascular system itself might be a critical factor contributing to salt sensitivity. In our previous studies, we reported an increased expression of TRPC3 in hypertensive subjects, and the increased expression of TRPC3 resulted in spontaneous hypertension through modulating the intracellular calcium overload.<sup>24–27</sup> TRPC3 overexpression enhanced carotid artery contractility by facilitating Ca<sup>2+</sup> and Na<sup>+</sup> influx.<sup>51</sup> In this study, we provide evidence to identify TRPC3 as an important salt-sensitive channel that causes calcium overload in VSMCs and subsequent vasoconstriction. In addition to the increased expression in vasculature, overexpression of TRPC3 directly mimicked the effect of HS diet that stimulated vasoconstriction, whereas inhibition or knockout of TRPC3 attenuated salt-induced vasoconstriction and hypertension. Also, we showed that canagliflozin might directly act on TRPC3 and inhibited both vascular TRPC3 expression and activity. Correspondingly, the antihypertensive effects of canagliflozin were diminished by inhibition or knockdown of TRPC3. This indicated that TRPC3 might be a crucial target of antihypertensive effect of canagliflozin. However, TRPC3



channel is more permeable to Na<sup>+</sup> versus Ca<sup>2+</sup> cations (nearly 6:1), and this channel is that inflow of Na<sup>+</sup> and small amounts of Ca<sup>2+</sup> that depolarizes the plasma membrane and opens voltage-dependent Ca<sup>2+</sup>

channel.<sup>52,53</sup> Thus, it is probable that mechanisms secondary to TRPC3-mediated Na<sup>+</sup> influx generate Ca<sup>2+</sup> signals leading to calcium overload in VSMCs and subsequent vasoconstriction.

**Figure 6. Canagliflozin reduced vasoconstriction by inhibiting high-salt-induced TRPC3-reverse mode NCX1 complexes.** **A**, Effects of SN6 (NCX1 pan inhibitor, 10  $\mu\text{mol/L}$ ) and pyr3 on U46619- and PE-induced vasoconstriction of the mesenteric artery rings isolated from wild-type mice.  $n=8$ . **B**,  $[\text{Ca}^{2+}]_{\text{cyt}}$  in ER  $\text{Ca}^{2+}$  release and  $\text{Ca}^{2+}$  uptake in mouse VSMCs transferred with TRPC3-oe and si-TRPC3 plasmids and treated with control, HS, SN6 (10  $\mu\text{mol/L}$  SN6), and HS+SN6 (20 mmol/L NaCl+10  $\mu\text{mol/L}$  SN6). The quantitative results are shown on the right.  $n=12$ . **C**, The relative protein expression levels of NCX1 in mouse VSMCs transferred with TRPC3-nc, TRPC3-oe and si-TRPC3 plasmids and treated with control (Con), HS, and HS+canagliflozin (HS+Cana). **D**, Effects of SN6 and KB-R7943 (reverse mode NCX1 inhibitor, 10  $\mu\text{mol/L}$ ) on U46619- or PE-induced vasoconstriction of the mesenteric artery rings isolated from wild-type mice fed with high-salt diet.  $n=8$ . **E** and **F**,  $[\text{Ca}^{2+}]_{\text{cyt}}$  in ER  $\text{Ca}^{2+}$  release and  $\text{Ca}^{2+}$  uptake in mouse VSMCs transferred with TRPC3oe and si-TRPC3 plasmids and treated with control, HS, KB-R7943 (10  $\mu\text{mol/L}$  KB-R7943), and HS+KB-R7943 (20 mmol/L NaCl+10  $\mu\text{mol/L}$  KB-R7943). The quantitative results are shown on the right.  $n=12$ . **G** and **H**, Effects of SN6 and KB-R7943 on U46619- and PE-induced vasoconstriction of the mesenteric artery rings isolated from wild-type and TRPC3<sup>-/-</sup> mice fed with high-salt diet.  $n=8$ . **I**,  $[\text{Ca}^{2+}]_{\text{cyt}}$  in ER  $\text{Ca}^{2+}$  release and  $\text{Ca}^{2+}$  uptake in mouse VSMCs treated with HS, HS+canagliflozin, pyr3+canagliflozin (20 mmol/L NaCl+10  $\mu\text{mol/L}$  pyr3+10  $\mu\text{mol/L}$  canagliflozin), KB-R7943+canagliflozin (20 mmol/L NaCl+10  $\mu\text{mol/L}$  KB-R7943+10  $\mu\text{mol/L}$  canagliflozin), and pyr3+KB-R7943 (20 mmol/L NaCl+10  $\mu\text{mol/L}$  pyr3+10  $\mu\text{mol/L}$  KB-R7943). The quantitative results are shown on the right.  $n=12$ . **J**, The relative mRNA expression levels of TRPC3 and NCX1 in VSMCs treated with control, HS, HS+canagliflozin, HS+pyr3, HS+SN6, and HS+KB-R7943.  $n=8$ . **K**, Input and Immunoprecipitation of TRPC3 and NCX1 in VSMCs and immunoblotted by TRPC3 and NCX1 antibody.  $n=8$ . Results are expressed as mean $\pm$ SEM. Statistical significance was determined by unpaired Student *t* test for comparisons between 2 groups and 1-way ANOVA followed by Bonferroni's posttest for multiple comparisons. \* $P<0.05$ , \*\* $P<0.01$ , \*\*\* $P<0.001$ , ns, no significance. Cana indicates canagliflozin; Con, control; ER indicates endoplasmic reticulum; HS, high-salt diet; Kb, KB-R7943; NCX1, sodium-calcium exchanger 1; ND, normal diet; PE, phenylephrine; si-TRPC3, TRPC3 silence; TRPC3, transient receptor potential channels 3; TRPC3-nc, TRPC3 negative control; TRPC3-oe, TRPC3 overexpression; and VSMC, vascular smooth muscle cell.

The vascular NCX1 involved in contraction of VSMCs has long been controversial. Overexpression of NCX1 is a main reason for the development of arrhythmias, heart failure, stroke, hypertension, etc.<sup>54</sup> However, mild increase of NCX1 expression in arteries promotes vasodilation in response to increased calcium efflux,<sup>55</sup> suggesting that the detrimental effect of NCX1 in cardiovascular diseases are not determined by its expression. It is widely accepted that NCX1 displays two modes of action to transfer  $\text{Ca}^{2+}$  either into or out of VSMCs in exchange for  $\text{Na}^+$  (3  $\text{Na}^+$ :1  $\text{Ca}^{2+}$ ), namely the forward ( $\text{Ca}^{2+}$ -efflux) mode and the reverse ( $\text{Ca}^{2+}$ -influx) mode, and even a relatively small increase in  $\text{Na}^+$  flux can markedly change the driving force of  $\text{Ca}^{2+}$  flux through NCX1.<sup>56,57</sup> Previous studies have shown the reverse mode of NCX1-mediated calcium overload as an essential factor for hypertension and results from the promotional effect of cytosolic  $\text{Na}^+$  rise on the activation of NCX1 reverse mode to facilitate  $\text{Ca}^{2+}$  entry.<sup>37,38,58–60</sup> However, the mechanism underlying the activation of NCX1 reverse mode remains unclear. In the present study, we showed a significant increase of NCX1 expression in response to salt loading, and its expression level increased in both SS and SS-19<sup>BN</sup>, indicating that the expression increase of NCX1 was not necessary to salt-sensitive hypertension. Surprisingly, we noticed that the switching of the reverse mode of NCX1 required the presence of TRPC3, as evidenced by the effect of NCX1 reverse mode inhibitor KB-R7943 on salt-induced VSMCs calcium influx or vascular contraction was blocked by knockdown or knockout of TRPC3, suggesting that TRPC3 might promote vasoconstriction and hypertension by facilitating the activation of the

reverse mode of NCX1. A rise in  $[\text{Ca}^{2+}]_{\text{cyt}}$  in VSMCs is an important stimulus for cell contraction, migration, and proliferation. Indeed, treatment of human VSMCs with KB-R7943 also inhibited cell proliferation in the presence of serum and growth factors.<sup>61,62</sup> Thus, the promotional effect of TRPC3 on NCX1-mediated calcium uptake would also be a critical reason for the increased vascular remodeling upon salt loading. In addition, the augmented interaction between TRPC3 and NCX1 in response to high salt intake implies that their interaction might be critical for the activation of the reverse mode of NCX1. Meanwhile, our study revealed that canagliflozin inhibited the activation of the reverse mode of NCX1 by specifically inhibiting TRPC3, thereby inhibiting cytoplasmic calcium uptake and vasoconstriction. Therefore, we propose a possible explanation that high salt activated  $\text{Na}^+$  permeable TRPC3, leading to local  $\text{Na}^+$  accumulation and  $\text{Ca}^{2+}$  influx via NCX1. However, the specific sites and molecular mechanisms of protein interactions of TRPC3 on NCX1 still needs further investigation.

## CONCLUSIONS

In conclusion, this study identifies TRPC3 channel as a salt-sensitive cation channel that interacts with NCX1 to regulate vascular calcium handling. High-salt-induced hypertension is associated with TRPC3/NCX1 mediated dysfunction of vascular calcium handling, which can be remarkably improved by canagliflozin treatment. This effect of canagliflozin is beyond its classic action and would represent a novel strategy to antagonize high salt jeopardizing and salt-sensitive hypertension.

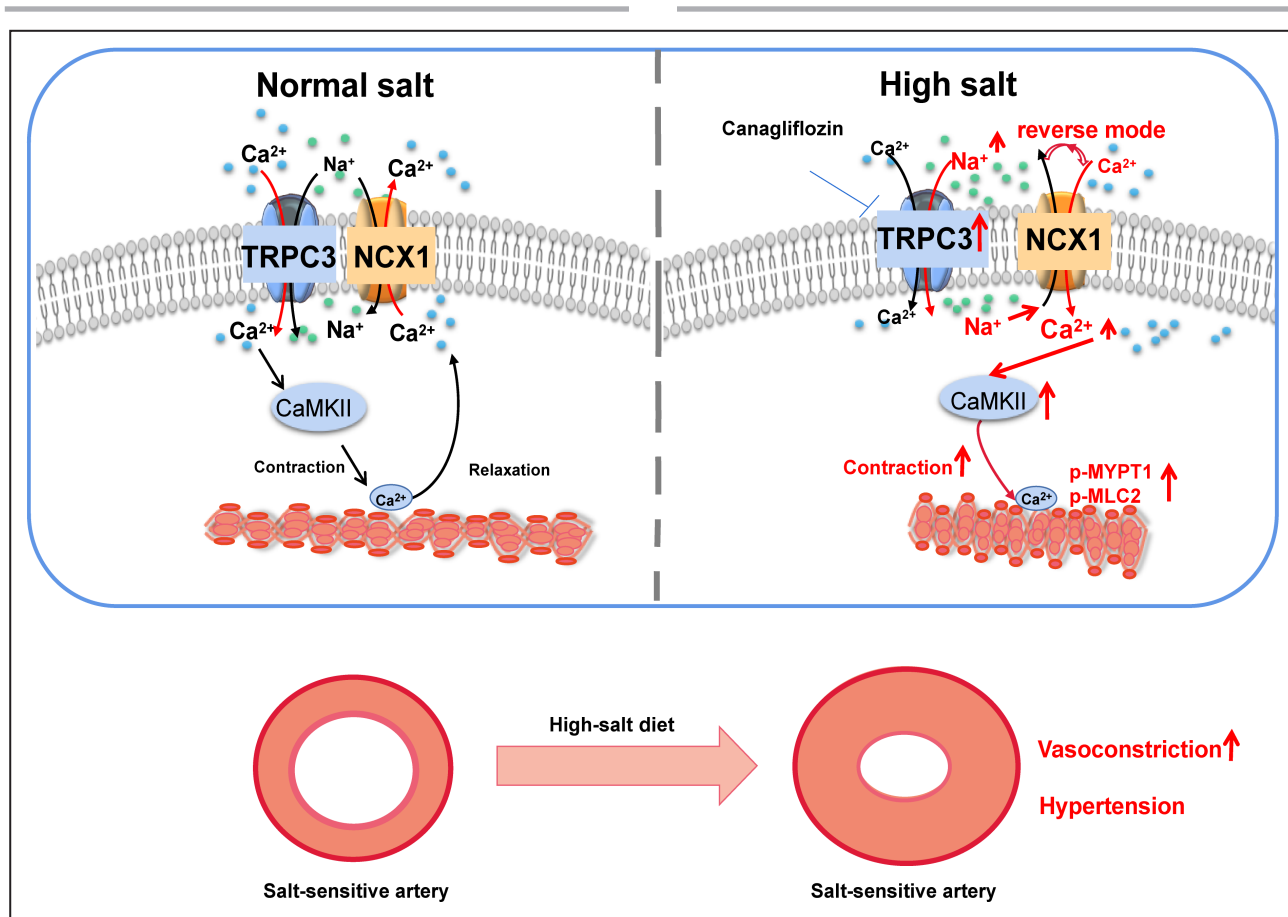


**Figure 7. Schematic diagram of this work.**

TRPC3 and NCX1 maintain dynamic calcium balance and participate in vascular activities under physiological conditions. However, upregulation of TRPC3 by high salt leads to intracellular Na<sup>+</sup> accumulation and then activated reverse mode of NCX1, which promotes sustained vasoconstriction caused by increased cytosolic calcium concentration. This might be an important reason for salt-sensitive hypertension. The antihypertensive effects of canagliflozin are mediated by decreasing cytosolic calcium concentration and vasoconstriction through inhibition of TRPC3. NCX1 indicates sodium-calcium exchanger 1; and TRPC3, transient receptor potential channels 3.

## ARTICLE INFORMATION

Received January 28, 2022; accepted April 29, 2022.

### Affiliation

Department of Hypertension and Endocrinology, Center for Hypertension and Metabolic Diseases, Daping Hospital, Army Medical University, Chongqing Institute of Hypertension, Chongqing, China

### Acknowledgments

We thank Yue Li, Huan Ma, Mei You, Qing Zhou, Bowen Wang and Aidi Mou (Chongqing Institute of Hypertension, China) for their technical assistance. We sincerely thank Hongfang Jin (Department of Pediatrics, Peking University First Hospital) for their technical assistance of the plasma H<sub>2</sub>S measurement.

### Sources of Funding

This study was supported by grants from the National Natural Science Foundation of China (81920108010, 91939102, 82022006, 81721001, 81630015, 82070441, 32000801 and 81670382).

### Disclosures

None.

### Supplemental Material

Tables S1–S2  
Figures S1–S4

## REFERENCES

- Benjamin EJ, Muntner P, Alonso A, Bittencourt MS, Callaway CW, Carson AP, Chamberlain AM, Chang AR, Cheng S, Das SR, et al. Heart disease and stroke statistics-2019 update: a report from the American Heart Association. *Circulation*. 2019;139:e56–e528. doi: 10.1161/CIR.0000000000000659
- Messerli FH, Hofstetter L, Syrogiannouli L, Rexhaj E, Siontis GCM, Seiler C, Bangalore S. Sodium intake, life expectancy, and all-cause mortality. *Eur Heart J*. 2021;42:2103–2112. doi: 10.1093/eurheartj/ehaa947
- Rossetto G, Maiolino G, Lerco S, Ceolotto G, Blackburn G, Mary S, Antonelli G, Berton C, Bisogni V, Cesari M, et al. High sodium intake, glomerular hyperfiltration, and protein catabolism in patients with essential hypertension. *Cardiovasc Res*. 2021;117:1372–1381. doi: 10.1093/cvr/cvaa205
- Fujita T. Mechanism of salt-sensitive hypertension: focus on adrenal and sympathetic nervous systems. *J Am Soc Nephrol*. 2014;25:1148–1155. doi: 10.1681/ASN.2013121258
- Neal B, Wu Y, Feng X, Zhang R, Zhang Y, Shi J, Zhang J, Tian M, Huang L, Li Z, et al. Effect of salt substitution on cardiovascular events and death. *N Engl J Med*. 2021;385:1067–1077. doi: 10.1056/NEJMoa2105675
- Powles J, Fahimi S, Micha R, Khatibzadeh S, Shi P, Ezzati M, Engell RE, Lim SS, Danaei G, Mozaffarian D. Global, regional and national sodium intakes in 1990 and 2010: a systematic analysis of 24 h urinary sodium excretion and dietary surveys worldwide. *BMJ Open*. 2013;3:e003733. doi: 10.1136/bmjopen-2013-003733



7. McGuire DK, Zinman B, Inzucchi SE, Wanner C, Fitchett D, Anker SD, Pocock S, Kaspers S, George JT, von Eynatten M, et al. Effects of empagliflozin on first and recurrent clinical events in patients with type 2 diabetes and atherosclerotic cardiovascular disease: a secondary analysis of the EMPA-REG OUTCOME trial. *Lancet Diabetes Endocrinol.* 2020;8:949–959. doi: 10.1016/S2213-8587(20)30344-2
8. Perkovic V, de Zeeuw D, Mahaffey KW, Fulcher G, Erondy N, Shaw W, Barrett TD, Weidner-Wells M, Deng H, Matthews DR, et al. Canagliflozin and renal outcomes in type 2 diabetes: results from the CANVAS Program randomised clinical trials. *Lancet Diabetes Endocrinol.* 2018;6:691–704. doi: 10.1016/S2213-8587(18)30141-4
9. Neuen BL, Oshima M, Perkovic V, Agarwal R, Arnott C, Bakris G, Cannon CP, Charytan DM, Edwards R, Górriz JL, et al. Effects of canagliflozin on serum potassium in people with diabetes and chronic kidney disease: the CREDENCE trial. *Eur Heart J.* 2021;42:4891–4901. doi: 10.1093/eurheartj/ehab497
10. Oyama K, Raz I, Cahn A, Kuder J, Murphy SA, Bhatt DL, Leiter LA, McGuire DK, Wilding JPH, Park KS, et al. Obesity and effects of dapagliflozin on cardiovascular and renal outcomes in patients with type 2 diabetes mellitus in the DECLARE-TIMI 58 trial. *Eur Heart J.* 2021 Aug 24;ehab530. doi: 10.1093/eurheartj/ehab530
11. Imran H, Nester W, Elgendy I, Saad M. Role of sodium glucose cotransporter 2 inhibitors in patients with heart failure: an elusive mechanism. *Ann Med.* 2020;52:178–190. doi: 10.1080/07853890.2020.1767298
12. Yamamura A, Yamamura H, Guo Q, Zimnicka AM, Wan J, Ko EA, Smith KA, Pohl NM, Song S, Zeifman A, et al. Dihydropyridine Ca(2+) channel blockers increase cytosolic [Ca(2+)] by activating Ca(2+)-sensing receptors in pulmonary arterial smooth muscle cells. *Circ Res.* 2013;112:640–650. doi: 10.1161/CIRCRESAHA.113.300897
13. Qian Q, Hunter L, Du H, Ren Q, Han Y, Sleck G. Pkd2+/- vascular smooth muscles develop exaggerated vasoconstriction in response to phenylephrine stimulation. *J Am Soc Nephrol.* 2007;18:485–493. doi: 10.1681/ASN.2006050501
14. Simo-Cheyrou E, Tan J, Grygorczyk R, Srivastava A. STIM-1 and ORAI-1 channel mediate angiotensin-II-induced expression of Egr-1 in vascular smooth muscle cells. *J Cell Physiol.* 2017;232:3496–3509. doi: 10.1002/jcp.25810
15. Touyz RM, Alves-Lopes R, Rios FJ, Camargo LL, Anagnostopoulou A, Arner A, Montezano AC. Vascular smooth muscle contraction in hypertension. *Cardiovasc Res.* 2018;114:529–539. doi: 10.1093/cvr/cvy023
16. Liu B, Zhang B, Huang S, Yang L, Roos CM, Thompson MA, Prakash YS, Zang J, Miller JD, Guo R. Ca entry through reverse mode Na/Ca exchanger contributes to store operated channel-mediated neointima formation after arterial injury. *Can J Cardiol.* 2018;34:791–799. doi: 10.1016/j.cjca.2018.01.012
17. Zhang B, Liu B, Roos CM, Thompson MA, Prakash YS, Miller JD, Guo RW. TRPC6 and TRPC4 heteromultimerization mediates store depletion-activated NCX1 reversal in proliferative vascular smooth muscle cells. *Channels.* 2018;12:119–125. doi: 10.1080/19336950.2018.1451696
18. Pulina MV, Zulian A, Baryshnikov SG, Linde CI, Karashima E, Hamlyn JM, Ferrari P, Blaustein MP, Golovina VA. Cross talk between plasma membrane Na(+)/Ca(2+) exchanger-1 and TRPC/Orai-containing channels: key players in arterial hypertension. *Adv Exp Med Biol.* 2013;961:365–374.
19. Álvarez-Miguel I, Ciudad P, Pérez-García M, López-López J. Differences in TRPC3 and TRPC6 channels assembly in mesenteric vascular smooth muscle cells in essential hypertension. *J Physiol.* 2017;595:1497–1513. doi: 10.1113/JP273327
20. Abdoul-Azize S, Buquet C, Vannier J, Dubus I. Pyr3, a TRPC3 channel blocker, potentiates dexamethasone sensitivity and apoptosis in acute lymphoblastic leukemia cells by disturbing Ca(2+) signaling, mitochondrial membrane potential changes and reactive oxygen species production. *Eur J Pharmacol.* 2016;784:90–98. doi: 10.1016/j.ejphar.2016.05.014
21. Senadheera S, Bertrand PP, Grayson TH, Leader L, Tare M, Murphy TV, Sandow SL. Enhanced contractility in pregnancy is associated with augmented TRPC3, L-type, and T-type voltage-dependent calcium channel function in rat uterine radial artery. *Am J Physiol Regul Integr Comp Physiol.* 2013;305:R917–R926. doi: 10.1152/ajpregu.00225.2013
22. Adebijoyi A, Thomas-Gatewood C, Leo M, Kidd M, Neeb Z, Jaggar J. An elevation in physical coupling of type 1 inositol 1,4,5-trisphosphate (IP3) receptors to transient receptor potential 3 (TRPC3) channels constricts mesenteric arteries in genetic hypertension. *Hypertension.* 2012;60:1213–1219. doi: 10.1161/HYPERTENSIONAHA.112.198820
23. Adebijoyi A, Zhao G, Narayanan D, Thomas-Gatewood C, Bannister J, Jaggar J. Isoform-selective physical coupling of TRPC3 channels to IP3 receptors in smooth muscle cells regulates arterial contractility. *Circ Res.* 2010;106:1603–1612. doi: 10.1161/CIRCRESAHA.110.216804
24. Wang B, Xiong S, Lin S, Xia W, Li Q, Zhao Z, Wei X, Lu Z, Wei X, Gao P, et al. Enhanced mitochondrial transient receptor potential channel, canonical type 3-mediated calcium handling in the vasculature from hypertensive rats. *J Am Heart Assoc.* 2017;6:e005812. doi: 10.1161/JAHA.117.005812
25. Liu D, Yang D, He H, Chen X, Cao T, Feng X, Ma L, Luo Z, Wang L, Yan Z, et al. Increased transient receptor potential canonical type 3 channels in vasculature from hypertensive rats. *Hypertension.* 2009;53:70–76. doi: 10.1161/HYPERTENSIONAHA.108.116947
26. Hu Y, Xia W, Li Y, Wang Q, Lin S, Wang B, Zhou C, Cui Y, Jiang Y, Pu X, et al. High-salt intake increases TRPC3 expression and enhances TRPC3-mediated calcium influx and systolic blood pressure in hypertensive patients. *Hypertens Res.* 2020;43:679–687. doi: 10.1038/s41440-020-0409-1
27. Ma T, Lin S, Wang B, Wang Q, Xia W, Zhang H, Cui Y, He C, Wu H, Sun F, et al. TRPC3 deficiency attenuates high salt-induced cardiac hypertrophy by alleviating cardiac mitochondrial dysfunction. *Biochem Biophys Res Commun.* 2019;519:674–681. doi: 10.1016/j.bbrc.2019.09.018
28. Yu H, Yang T, Gao P, Wei X, Zhang H, Xiong S, Lu Z, Li L, Wei X, Chen J, et al. Caffeine intake antagonizes salt sensitive hypertension through improvement of renal sodium handling. *Sci Rep.* 2016;6:25746. doi: 10.1038/srep25746
29. Xu D, Murakoshi N, Tajiri K, Duo F, Okabe Y, Murakata Y, Yuan Z, Li S, Aonuma K, Song Z, et al. Xanthine oxidase inhibitor febuxostat reduces atrial fibrillation susceptibility by inhibition of oxidized CAMKII in Dahl salt-sensitive rats. *Clin Sci.* 2021;135:2409–2422. doi: 10.1042/CS20210405
30. Sun L, Jin H, Sun L, Chen S, Huang Y, Liu J, Li Z, Zhao M, Sun Y, Tang C, et al. Hydrogen sulfide alleviates myocardial collagen remodeling in association with inhibition of TGF-β/Smad signaling pathway in spontaneously hypertensive rats. *Mol Med.* 2015;20:503–515. doi: 10.2119/molmed.2013.00096
31. Brun BF, Strela FB, Berger RCM, Melo SFS, de Oliveira EM, Barauna VG, Vassallo PF. Blockade of AT1 receptor restore the migration of vascular smooth muscle cells in high sodium medium. *Cell Biol Int.* 2019;43:890–898. doi: 10.1002/cbin.11162
32. Liu Y, Xing J, Li Y, Luo Q, Su Z, Zhang X, Zhang H. Circpchronic hypoxia-induced hypermethylation attenuates hypothermic cardioprotection via down-regulation of ubiquitinone biosynthesis. *Sci Transl Med.* 2019;11:eaat8406. doi: 10.1126/scitranslmed.aat8406
33. Huang X, Yi S, Hu J, Du Z, Wang Q, Ye Z, Cao Q, Su G, Yuan G, Zhou C, et al. Analysis of the role of palmitoleic acid in acute anterior uveitis. *Int Immunopharmacol.* 2020;84:106552. doi: 10.1016/j.intimp.2020.106552
34. Zhou Q, Xie F, Zhou B, Wang J, Wu B, Li L, Kang Y, Dai R, Jiang Y. Differentially expressed proteins identified by TMT proteomics analysis in bone marrow microenvironment of osteoporotic patients. *Osteoporos Int.* 2019;30:1089–1098. doi: 10.1007/s00198-019-04884-0
35. Limbu R, Cottrell G, McNeish A. Characterisation of the vasodilation effects of DHA and EPA, n-3 PUFAs (fish oils), in rat aorta and mesenteric resistance arteries. *PLoS One.* 2018;13:e0192484. doi: 10.1371/journal.pone.0192484
36. Wei X, Wei X, Lu Z, Li L, Hu Y, Sun F, Jiang Y, Ma H, Zheng H, Yang G, et al. Activation of TRPV1 channel antagonizes diabetic nephropathy through inhibiting endoplasmic reticulum-mitochondria contact in podocytes. *Metabolism.* 2020;105:154182. doi: 10.1016/j.metabol.2020.154182
37. Puleo F, Kim K, Frame AA, Walsh KR, Ferdaus MZ, Moreira JD, Comsti E, Faudoa E, Nist KM, Abkin E, et al. Sympathetic regulation of the NCC (sodium chloride cotransporter) in Dahl salt-sensitive hypertension. *Hypertension.* 2020;76:1461–1469. doi: 10.1161/HYPERTENSIONAHA.120.15928
38. Iwamoto T, Kita S, Zhang J, Blaustein MP, Arai Y, Yoshida S, Wakimoto K, Komuro I, Katsuragi T. Salt-sensitive hypertension is triggered by Ca<sup>2+</sup> entry via Na<sup>+</sup>/Ca<sup>2+</sup> exchanger type-1 in vascular smooth muscle. *Nat Med.* 2004;10:1193–1199. doi: 10.1038/nm1118
39. Lu Z, Cui Y, Wei X, Gao P, Zhang H, Wei X, Li Q, Sun F, Yan Z, Zheng H, et al. Deficiency of PKD2L1 (TRPP3) exacerbates pathological cardiac hypertrophy by augmenting NCX1-mediated mitochondrial calcium overload. *Cell Rep.* 2018;24:1639–1652. doi: 10.1016/j.celrep.2018.07.022
40. Hallow K, Gebremichael Y. A quantitative systems physiology model of renal function and blood pressure regulation: application in salt-sensitive

- hypertension. *CPT Pharmacometrics Syst Pharmacol*. 2017;6:393–400. doi: 10.1002/psp4.12177
41. Majid D, Prieto M, Navar L. Salt-sensitive hypertension: perspectives on intrarenal mechanisms. *Curr Hypertens Rev*. 2015;11:38–48. doi: 10.2174/1573402111666150530203858
  42. Armando I, Villar V, Jose P. Genomics and pharmacogenomics of salt-sensitive hypertension. *Curr Hypertens Rev*. 2015;11:49–56. doi: 10.2174/1573402111999150521102331
  43. Potter JC, Whiles SA, Miles CB, Whiles JB, Mitchell MA, Biederman BE, Dawoud FM, Breuel KF, Williamson GA, Picken MM, et al. Salt-sensitive hypertension, renal injury, and renal vasodysfunction associated with Dahl salt-sensitive rats are abolished in consomic SS.BN1 rats. *J Am Heart Assoc*. 2021;10:e020261. doi: 10.1161/JAHA.120.020261
  44. Cowie M, Fisher M. SGLT2 inhibitors: mechanisms of cardiovascular benefit beyond glycaemic control. *Nat Rev Cardiol*. 2020;17:761–772. doi: 10.1038/s41569-020-0406-8
  45. Cherney DZI, Dekkers CCJ, Barbour SJ, Cattran D, Abdul Gafor AH, Greasley PJ, Laverman GD, Lim SK, Di Tanna GL, Reich HN, et al. Effects of the SGLT2 inhibitor dapagliflozin on proteinuria in non-diabetic patients with chronic kidney disease (DIAMOND): a randomised, double-blind, crossover trial. *Lancet Diabetes Endocrinol*. 2020;8:582–593. doi: 10.1016/S2213-8587(20)30162-5
  46. Santos-Gallego CG, Requena-Ibanez JA, San Antonio R, Garcia-Ropero A, Ishikawa K, Watanabe S, Picatoste B, Vargas-Delgado AP, Flores-Umanzor EJ, Sanz J, et al. Empagliflozin ameliorates diastolic dysfunction and left ventricular fibrosis/stiffness in nondiabetic heart failure: a multimodality study. *JACC Cardiovasc Imaging*. 2021;14:393–407. doi: 10.1016/j.jcmg.2020.07.042
  47. Durante W, Behnammanesh G, Peyton K. Effects of sodium-glucose co-transporter 2 inhibitors on vascular cell function and arterial remodeling. *Int J Mol Sci*. 2021;22:8786. doi: 10.3390/ijms22168786
  48. Yousaf Z, Munir W, Hammamy RAM. Use of SGLT-2 inhibitor in COVID-19: A cautionary tale. *MedComm*. 2021;2:114–116. doi: 10.1002/mco.2.45
  49. Solini A, Giannini L, Seghieri M, Vitolo E, Taddei S, Ghiadoni L, Bruno RM. Dapagliflozin acutely improves endothelial dysfunction, reduces aortic stiffness and renal resistive index in type 2 diabetic patients: a pilot study. *Cardiovasc Diabetol*. 2017;16:138. doi: 10.1186/s12933-017-0621-8
  50. Korkmaz-Icöz S, Kocer C, Sayour AA, Kraft P, Benker MI, Abulizi S, Georgevici AI, Brlecic P, Radovits T, Loganathan S, et al. The sodium-glucose cotransporter-2 inhibitor canagliflozin alleviates endothelial dysfunction following in vitro vascular ischemia/reperfusion injury in rats. *Int J Mol Sci*. 2021;22:7774. doi: 10.3390/ijms22157774
  51. Noorani M, Noel R, Marrelli S. Upregulated TRPC3 and downregulated TRPC1 channel expression during hypertension is associated with increased vascular contractility in rat. *Front Physiol*. 2011;2:42. doi: 10.3389/fphys.2011.00042
  52. Pires P, Earley S. A TRPC3 signalling complex promotes cerebral artery remodelling during hypertension. *Cardiovasc Res*. 2016;109:4–5. doi: 10.1093/cvr/cvv261
  53. Andrikopoulos P, Eccles S, Yaqoob M. Coupling between the TRPC3 ion channel and the NCX1 transporter contributed to VEGF-induced ERK1/2 activation and angiogenesis in human primary endothelial cells. *Cell Signal*. 2017;37:12–30. doi: 10.1016/j.cellsig.2017.05.013
  54. Khananshvilii D. Sodium-calcium exchangers (NCX): molecular hallmarks underlying the tissue-specific and systemic functions. *Pflugers Arch*. 2014;466:43–60. doi: 10.1007/s00424-013-1405-y
  55. Wang Y, Zhang J, Wier W, Chen L, Blaustein M. NO-induced vasodilation correlates directly with BP in smooth muscle-Na/Ca exchanger-1-engineered mice: elevated BP does not attenuate endothelial function. *Am J Physiol Heart Circ Physiol*. 2021;320:H221–H237. doi: 10.1152/ajpheart.00487.2020
  56. Blaustein M, Lederer W. Sodium/calcium exchange: its physiological implications. *Physiol Rev*. 1999;79:763–854. doi: 10.1152/physrev.1999.79.3.763
  57. Rose C, Ziemens D, Verkhatsky A. On the special role of NCX in astrocytes: translating Na-transients into intracellular Ca signals. *Cell Calcium*. 2020;86:102154. doi: 10.1016/j.ceca.2019.102154
  58. Burr AR, Millay DP, Goonasekera SA, Park KH, Sargent MA, Collins J, Altamirano F, Philipson KD, Allen PD, Ma J, et al. Na<sup>+</sup> dysregulation coupled with Ca<sup>2+</sup> entry through NCX1 promotes muscular dystrophy in mice. *Mol Cell Biol*. 2014;34:1991–2002. doi: 10.1128/MCB.00339-14
  59. Rahman M, Inman M, Kiss L, Janssen L. Reverse-mode NCX current in mouse airway smooth muscle: Na<sup>(+)</sup> and voltage dependence, contributions to Ca<sup>(2+)</sup> influx and contraction, and altered expression in a model of allergen-induced hyperresponsiveness. *Acta Physiol*. 2012;205:279–291. doi: 10.1111/j.1748-1716.2011.02401.x
  60. Yamamura K, Tani M, Hasegawa H, Gen W. Very low dose of the Na<sup>(+)</sup>/Ca<sup>(2+)</sup> exchange inhibitor, KB-R7943, protects ischemic reperfused aged Fischer 344 rat hearts: considerable strain difference in the sensitivity to KB-R7943. *Cardiovasc Res*. 2001;52:397–406. doi: 10.1016/S0008-6363(01)00409-6
  61. Zhang S, Yuan J, Barrett K, Dong H. Role of Na<sup>+</sup>/Ca<sup>2+</sup> exchange in regulating cytosolic Ca<sup>2+</sup> in cultured human pulmonary artery smooth muscle cells. *Am J Physiol Cell Physiol*. 2005;288:C245–C252. doi: 10.1152/ajpcell.00411.2004
  62. Raizman JE, Komljenovic J, Chang R, Deng C, Bedosky KM, Rattan SG, Cunningham RH, Freed DH, Dixon IM. The participation of the Na<sup>+</sup>-Ca<sup>2+</sup> exchanger in primary cardiac myofibroblast migration, contraction, and proliferation. *J Cell Physiol*. 2007;213:540–551. doi: 10.1002/jcp.21134

# **SUPPLEMENTAL MATERIAL**

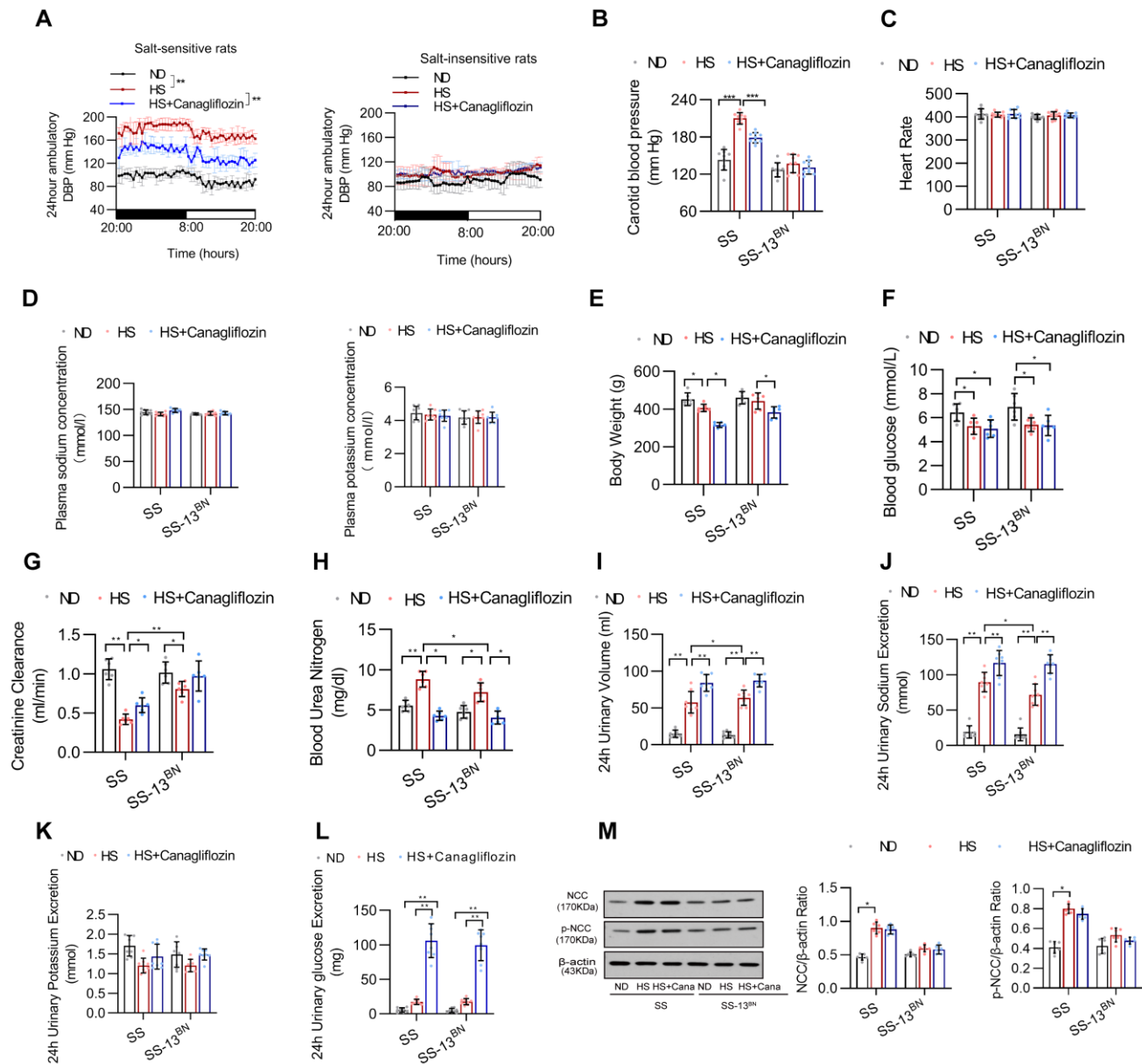
**Table S1. Animals (in vivo studies).**

<b>Species</b>	<b>Vendor or Source</b>	<b>Background Strain</b>	<b>Sex</b>
TRPC3 knockout mice	Jackson Laboratory (Bar Harbor, ME)	129S2	Male
Wild-type mice	Jackson Laboratory (Bar Harbor, ME)	129S2	Male
Dahl salt-sensitive rats	Vital River Company (Beijing, China)	Sprague Dawley	Male
Dahl salt-insensitive rats	Vital River Company (Beijing, China)	Sprague Dawley	Male

**Table S2. Antibodies.**

<b>Target antigen</b>	<b>Vendor or Source</b>	<b>Catalog #</b>	<b>Working concentration</b>	<b>Lot # (preferred but not required)</b>
TRPC3	alomone	ACC-016	1:500	
NCX1	Abcam	ab177952	1:500	
CaMKII	Abcam	ab134041	1:500	
Phospho-CaMKII	CST	12716S	1:500	
MYPT1	Santa Cruz	514261	1:500	
Phospho-MYPT1	Santa Cruz	33360	1:500	
MLC2	CST	3672	1:500	
Phospho- MLC2	CST	3675	1:500	
NCX1	Proteintech	55075-1-AP	1:500	

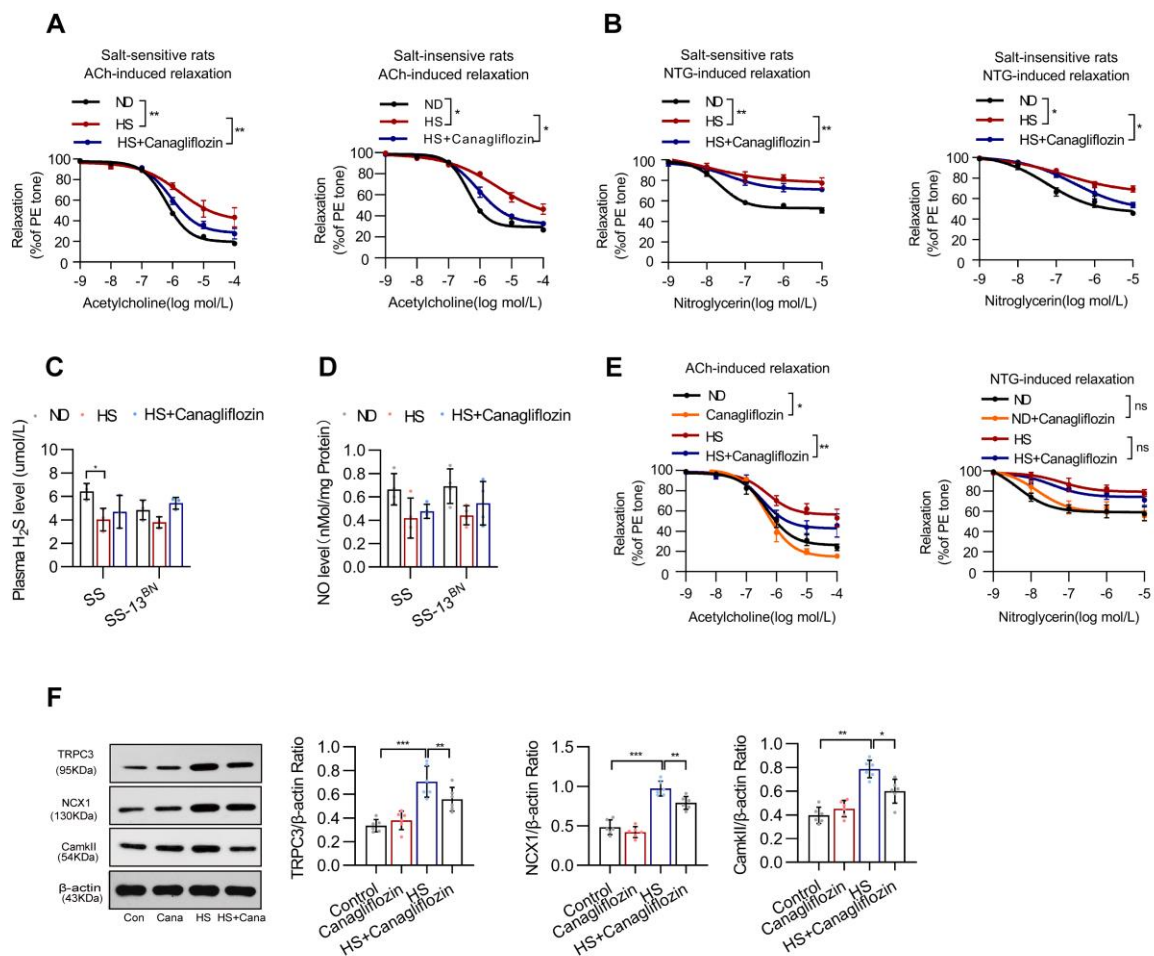
**Figure S1. The metabolic effects and blood pressure of canagliflozin in Dahl salt-sensitive and Dahl salt-insensitive rats. Related to Figure 1.**



(A) DBP from twenty-four-hour blood pressure was determined using radiotelemetry at 12<sup>th</sup> week in Dahl salt-sensitive and Dahl salt-insensitive rats. n=6. (B) The carotid blood pressure at 12<sup>th</sup> week in Dahl salt-sensitive and Dahl salt-insensitive rats fed with ND, HS and HS+ canagliflozin. n=6. SS, Dahl salt-sensitive; SS-13<sup>BN</sup>, Dahl salt-insensitive rats. (C) The heart rate of the Dahl salt-sensitive and Dahl salt-insensitive rats. n=8. (D) The plasma sodium concentration and the plasma potassium concentration of the Dahl salt-sensitive and Dahl salt-insensitive rats. n=8. (E and F) The body weight and the blood glucose of the Dahl salt-sensitive and Dahl salt-insensitive rats. \*P<0.05, n=8. (G and H) The creatinine clearance and the blood urea nitrogen of the Dahl salt-sensitive and Dahl salt-insensitive rats. n=8. (I) The twenty-four-hour urinary volume of the Dahl salt-sensitive and Dahl salt-insensitive rats. n=8. (J and K) The twenty-four-hour urinary

sodium excretion and urinary potassium excretion of the Dahl salt-sensitive and Dahl salt-insensitive rats. n=8. **(L)** The twenty-four-hour urinary glucose excretion of the Dahl salt-sensitive and Dahl salt-insensitive rats.n=8. **(M)** Representative western blots of NCC and phosphorylation of NCC (NCC) in kidney from Dahl salt-sensitive and Dahlsalt-insensitive rats fed with ND, HS and HS+canagliflozin(HS+Cana).  $\beta$ -actin served as a loading control.n=6. Data are expressed as mean  $\pm$  SEM. Statistical significance was determined by unpaired Student's t-test for comparisons between two groups and one-way ANOVA followed by Bonferroni's post-test for multiple comparisons. \*P<0.05, \*\*P<0.01, \*\*\*P<0.001. SS, Dahl salt-sensitive rats;SS-13<sup>BN</sup>, Dahl salt-insensitive rats.

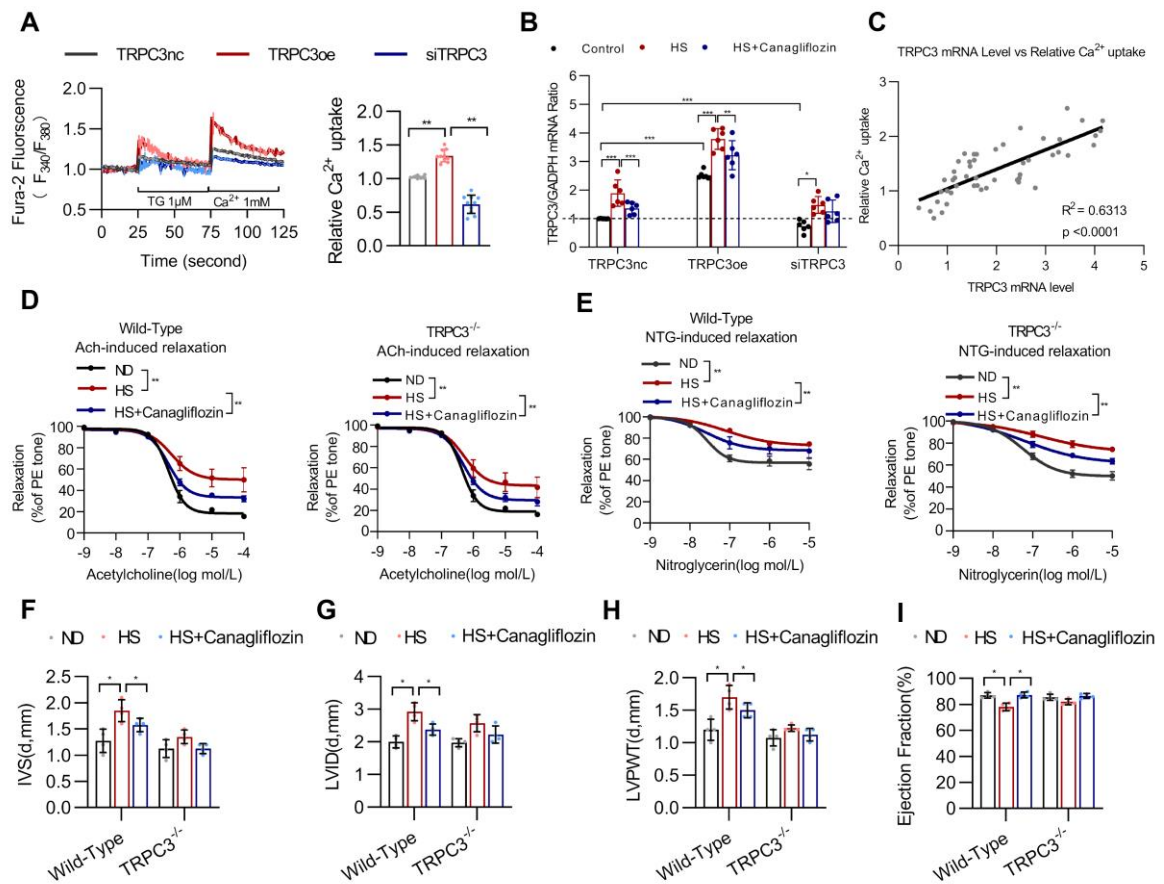
**Figure S2. The direct effect of canagliflozin on vasodilation in Dahl salt-sensitive rats. Related to Figure 2 and 3.**



(A) Endothelium-dependent relaxations of the mesenteric artery rings from Dahl salt-sensitive and Dahl salt-insensitive rats. n=6. (B) Endothelium-independent relaxations of the mesenteric artery rings from Dahl salt-sensitive and Dahl salt-insensitive rats. n=6. (C) The plasma H<sub>2</sub>S levels of of the Dahl salt-sensitive and Dahl salt-insensitive rats. n=3. (D) The aortic NO levels of the Dahl salt-sensitive and Dahl salt-insensitive rats. n=4. (E) Effect of acute canagliflozin preincubation on endothelium-dependent or endothelium-independent vasodilation of the mesenteric artery rings from Dahl salt-sensitive rats. n=6. (F) Representative western blots of TRPC3, NCX1, CamkII in mouse VSMCs treated with control(Con), canagliflozin (Cana), HS and HS+canagliflozin (HS+Cana).  $\beta$ -actin served as a loading control. n=6. Data are expressed as mean  $\pm$  SEM. Statistical significance was determined by unpaired Student's t-test for comparisons between two groups and one-way ANOVA followed by Bonferroni's post-test for multiple comparisons. \*P<0.05, \*\*P<0.01, \*\*\*P<0.001, ns, no significance. SS, Dahl salt-sensitive rats; SS-13<sup>BN</sup>, Dahl salt-insensitive rats.

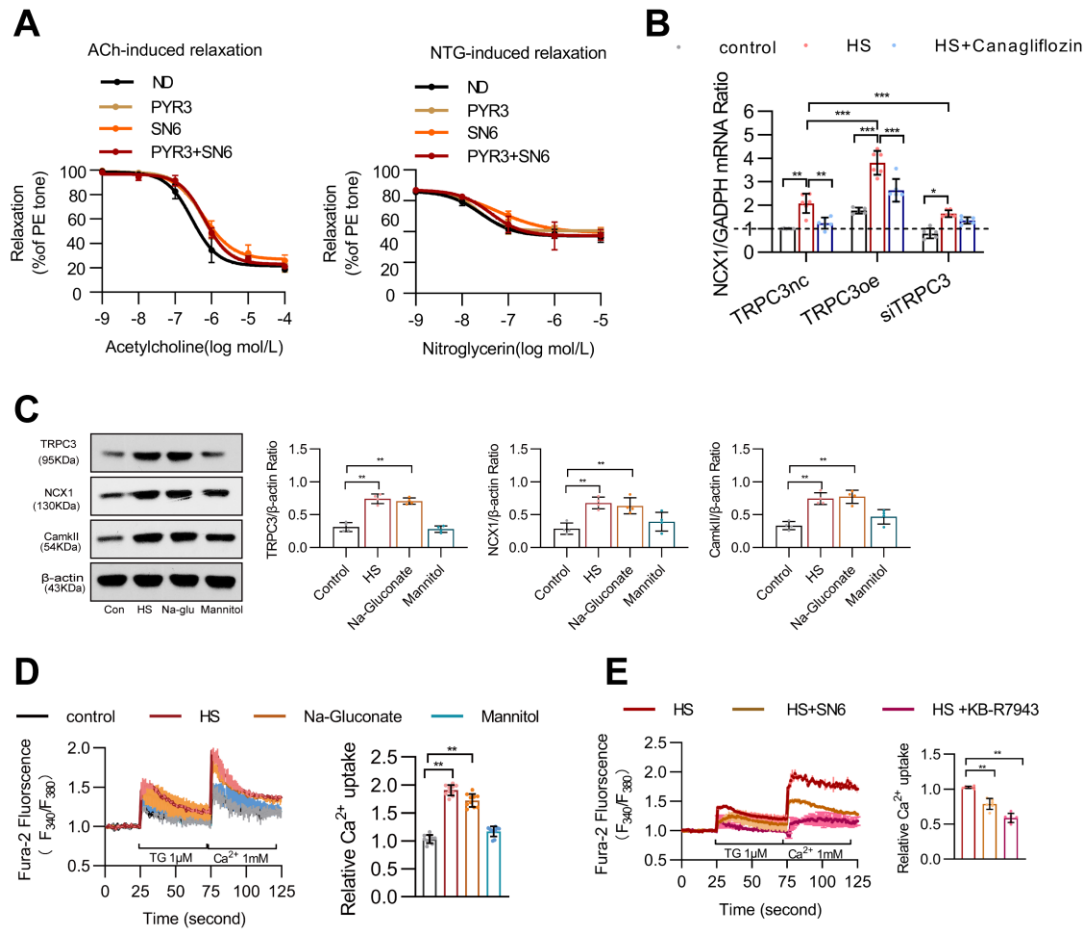


**FigureS3, The regulatory effects of TRPC3 on vasodilation and calcium uptake. Related to Figure 4 and 5.**



(A)  $[Ca^{2+}]_{cyt}$  in endoplasmic reticulum(ER) induced  $Ca^{2+}$  release and  $Ca^{2+}$  uptake in mouse VSMCs transferred with TRPC3-nc,TRPC3-oe and si-TRPC3 plasmids. The quantitative results are shown on the right. n=10. (B) The relative mRNA levels of TRPC3 in VSMCs transferred with TRPC3-nc, TRPC3-oe and si-TRPC3 plasmids and treated with control, HS and HS+canagliflozin. n=6. (C) The correlation between the TRPC3 mRNA level and the cytoplasmic calcium uptake. (D)The endothelium-dependent vasodilation of the mesenteric artery rings isolated from wild-type and TRPC3<sup>-/-</sup> mice. n=6. (E) The endothelium-independent vasodilation of the mesenteric artery rings isolated from wild-type and TRPC3<sup>-/-</sup> mice. n=6. (F) The interventricular septum in diastole of the wild-type and TRPC3<sup>-/-</sup> mice. n=4. (G) The left ventricular internal dimension in diastole of the wild-type and TRPC3<sup>-/-</sup> mice. n=4. (H) The posterior wall thickness of left ventricle in diastole of the wild-type and TRPC3<sup>-/-</sup> mice. n=4. (I) The ejection fraction of the wild-type and TRPC3<sup>-/-</sup> mice. n=4. Data are expressed as mean  $\pm$  SEM. Statistical significance was determined by unpaired Student's t-test for comparisons between two groups and one-way ANOVA followed by Bonferroni's post-test for multiple comparisons. The correlation were investigated by the linear regression analysis. \*P<0.05, \*\*P<0.01, \*\*\*P<0.001. TRPC3-nc, TRPC3 negative control; TRPC3-oe,TRPC3 overexpression; si-TRPC3, TRPC3 silence.

**FigureS4. The regulatory effects of TRPC3 and NCX1 on vasodilation and calcium uptake. Related to Figure 6.**



(A) Effects of SN6 and pyr3 on endothelium-dependent or endothelium-independent vasodilation of the mesenteric artery rings isolated from wild-type mice, n=6. (B) The relative mRNA expression levels of NCX1 in VSMCs transfected with TRPC3-nc, TRPC3-oe and si-TRPC3 plasmids and treated with control, HS and HS+canagliflozin. n=6. (C) Representative western blots of TRPC3, NCX1, CamkII in mouse VSMCs treated with control, HS, 40 mmol/L mannitol and 20 mmol/L Na-gluconate (Na-glu).  $\beta$ -actin served as a loading control. n=4. (D)  $[Ca^{2+}]_{cyt}$  in  $Ca^{2+}$  release and  $Ca^{2+}$  uptake in VSMCs treated with control, HS, mannitol and Na-gluconate. The quantitative results are shown on the right. n=10. (E)  $[Ca^{2+}]_{cyt}$  in  $Ca^{2+}$  release and  $Ca^{2+}$  uptake in VSMCs treated with HS, HS+SN6 and HS+KB-R7943. The quantitative results are shown on the right. n=6. Data are expressed as mean  $\pm$  SEM. Statistical significance was determined by unpaired Student's t-test for comparisons between two groups and one-way ANOVA followed by Bonferroni's post-test for multiple comparisons. \*P<0.05, \*\*P<0.01, \*\*\*P<0.001. TRPC3-nc, TRPC3 negative control; TRPC3-oe, TRPC3 overexpression; si-TRPC3, TRPC3 silence.